ISSN 1028-8546

Azərbaycan Milli Elmlər Akademiyası
Fizika-Riyaziyyat və Texnika Elmləri Bölməsi
Fizika İnstitutu

1

Fizika

Cild
VIII
2002

Bakı ✵ Elm

RADIATION STABLE ELECTROMECHANICAL TRANSFORMERS ON THE BASIS OF THREAD-LIKE MONOCRYSTALS Ge_{1-X} Si_X

M.K. KERIMOV, Sh.M. ABBASOV, Sh.I. ABBASOV
Radiation Research Department of Azerbaijan National Academy of Sciences
H.Javid ave. 31[a], Baku 370143.

The investigations of the electromechanical characteristics of the thread-like crystals Ge_{1-x} Si_x subjected to electron and γ- irradiation (Co^{60}) showed their increased radiation stability as compared with the other devices.

The results obtained allow to draw conclusion on perceptivity of application of the transformers based on thread-like monocrystals Ge_{1-x} Si_x for the practical realization of the automatization of the measurement process in different fields of engineering.

The advanced trend in the development of the measuring systems is the use of transformers (transmitters) based on a unique principle. As the experience in designing showed on the basis of the semiconductor thread-like monocrystals of silicon, germanium and $Ge_{1-x}Si_x$ the various types of the measuring transformers characterized by the constructive simplicity, high sensitivity and enlarged functional capability [1-3] could be created.

The unity of a principal solution and unification of devices is achieved due to creation of the base transformers (migrations on thermoresistors and deformations on thermoresistors), in which the sensitive elements are free monocrystals.

With reference to the development of thermoresistive transformers, it should be noted, that with all varieties of the constructions of this class transformers all of them contain a thermoresistor and a heater (thermowire) migrating one relatively another under the action of the parameter to be measured. As a rule, the thermoresistor is made, from the conductive material that eventually determines the construction and metrologic characteristics of the transformer.

The use of the thermoresistors from the semiconductor thread-like monocrystals 1 mm in length and 15 mcm in diameter allows to eliminate defects of the transformers with wire thermosensitive elements.

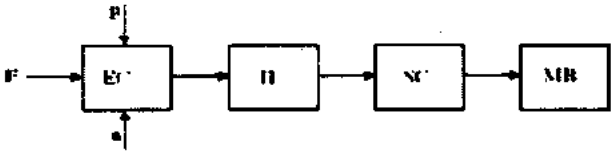

Fig. 1. Structural scheme of thermoresistive transformers.
EC – Elastic cell. H – Heater. SC – Sensitive cell.
MB – Measuring bringe.

The essence of the proposed method for transforming migration (or the other mechanical value, which can be put into migration) into an electrical signal consists of the possibility for local measurement of temperature by means of a miniature crystal. The transformer structural scheme (fig. 1) can be represented by the successive chain of links with the certain transforming functions and the corresponding error of components: the elastic cell (silphon) perceiving the measured value, cylindrical heater creating the required gradient of the temperature field along its axis; thermosensitive cell-thread-like crystal, mechanically connected with silphon by means of crystal holder and migrating inside the coaxially placed heater; measuring bridge with one or two active arms.

The analysis and calculation of such scheme allowed to determine the functional capabilities of the transformer, its mechanical and electrical parameters.

In the transformer of linear migrations the measuring rod is welded into the silphon- moving element which performs the migration of the crystal holder with the secured on the current outlets crystal relative to the immobile heater. In the given construction two variants of crystal arrangement (longitudinal and transverse) relative to the heater are possible.

By the investigations it was established that in the both cases the linear dependence of resistance change on migration occurs:

$$R(x)=R_o(1-\alpha Mx) \qquad (1)$$

where R_o is an initial resistance of a crystal; M is a coefficient characterizing the gradient of temperature in a heater; α is temperature coefficient of crystal resistance.

Under the action of the migration to be measured the crystal position inside a heater changes and thus its temperature and hence resistance which is transformed by the measuring scheme to analogous electrical signal change.

The transformer sensitivity is represented as

$$S=\frac{dR}{dx}=R_o\alpha\ M \qquad (2)$$

The high sensitivity by voltage allows to measure the output signal by the standard measuring device (digital voltmeter, potentiometer, self-recording device).

In the transformer of pressure the mechanical impact is perceived by the silphon itself which is connected with crystal holder. The inertia mass in the accelerometer is combined with silphon migrating relative to the heater under the action of acceleration.

In design of the thermoresistive transformers a number of the technological peculiarities which permit to decrease the measurement error have been taken into account. The investigations established that the measurement of the above parameters was performed with the main error in the order of 1–1.5%. The temperature error is 0.04%. The fast-response is within the range 0.1–0.3s. The significant advantage is the possibility for interchangeability of the transformers and their low cost.

The use of mechanical resonators opens new perspectives in creation of the tensoresistive transformers.

On the strength of all the properties such vibrating-frequency tensotransformers are the most advanced measuring means providing a number of advantages.

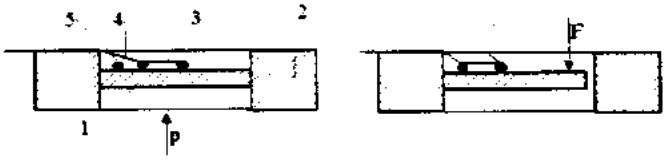

Fig. 2. Functional-schemes of vibro-frequency tensotransformers. 1-membrane; 2-supporting fillet; 3-crystal; 4-current-outlets; 5-excitation electrode.

The structural scheme of the transformer (fig. 2) includes: elastic cell transforming the mechanical value (force, pressure, acceleration) into string tension; oscillatory cell (resonator) – monocrystalline structure transforming the tension into the frequency of mechanical oscillations; exciting cell serving for excitation of the string mechanical oscillations; amplifier of the resonator electrical oscillations. In the proposed scheme the functions of the oscillatory and transforming units are combined in one cell – string from thread-like monocrystal. Due to this the direct transforming of the crystal mechanical oscillations to the electrical signal is effected at the expense of its internal properties.

The oscillation exciter as an individual cell is absent, for the oscillation excitation the elastic cell surface adjacent to the string is used.

The string tension is known to lead to the change of its own oscillations frequency and correspondingly to the change of the resistance variable component owing to the strain sensitivity. The relative resistance change is proportional to its deformation

$$\frac{\Delta R}{R} = KE \qquad (3)$$

where K is a coefficient of the crystal tensosensitivity.

If the direct current is passed through the string the tension pulsations will arise in it with frequency doubled with respect to the frequency of the mechanical oscillations. In general view the frequency of this tension can be determined by the formula [4]

$$f = \frac{1}{2l}\sqrt{\frac{\sigma}{\rho}} \qquad (4)$$

where l is a length of the string; σ is a tension of the stretching force acting on string; ρ is a density of the string material.

The functional schemes of vibrating-frequency tensotransformers of different purposes are presented in fig. 2.

In pressure transformer on silicic membrane with supporting fillet the thread-like $Ge_{1-x}Si_x$ monocrystal is rigidly secured in joints. The crystal current-outlets and electrical contact of the oscillations exciter are connected to more rigid contact outlets. In the transformer of forces and accelerometer the crystal is fasten on monocrystalline beam of the equal flexing resistance made by the method of ultrasonic treatment with subsequent chemical etching and polishing.

The maximum simplicity of the construction, consistensy of materials and junction in pick-up points allowed to achieve the high soundness of the string oscillations (10^5). The sensitivity to deformation reaches the value 10^9 Hz/per unit value.

The metrological estimate of the transformers by means of direct comparison with the exemplary measuring means gives the error value in the order of 0.01%. The important advantage of the given transformers is that their operation is not significantly affected by temperature dependencies of the tensosensitivity and resistance coefficient since the parameter to be measured is oscillation frequency which is determined by the crystal geometry, its mechanical properties and applied force.

The investigations of the electromechanical characteristics of the thread-like crystals $Ge_{1-x}Si_x$ subjected to electron and γ – irradiation (Co^{60}) showed their increased radiation stability as compared with Ge or Si crystals which considerably increased with increasing of silicium per cent content in a sample.

The results obtained allow to draw conclusion on perspectivity of application of the transformers based on thread-like monocrystals Ge – Si for the practical realization of the automatization of the measurement process in different fields of engineering.

[1] *R.I. Baitsar.* Pribori i technika eksperimenta. 1980, №3 (in Russian).
[2] Auth. Certif. 960634 USSR. Stringed resonator. B.I. №35. 1982.
[3] *Yu.G. Akhromenko, R.I. Baitsar, E.P. Krasnozhenov.* Phys. Elektronika. Lvov. 1985. Vip.31.
[4] *Sh.M. Abbasov, R.I. Baitsar, Sh.I. Abbasov, E.P. Krasnozhenov.* Izvestiya Natsion. Akad. Nauk Azerbaijana. 2000, v.20, №5, p.45-48.

M.K. Kərimov, Ş.M. Abbasov, Ş.İ. Abbasov

SAPŞƏKİLLİ $Ge_{1-x}Si_x$ MONOKRİSTALLARI ƏSASINDA RADİASİYAYADAVAMLI ELEKTROMEXANİKİ ÇEVİRİCİLƏR

Elektron və $\gamma(Co^{60})$ şüalarının təsirinə məruz qalmış sapşəkilli $Ge_{1-x}Si_x$ kristallarının elektromexaniki xassələrinin araşdırılması, onların radiasiyayadavamlılığının başqa cihazlara nisbətən daha yüksək olduğunu göstərmişdir.

Alınmış nəticələr sapşəkilli $Ge_{1-x}Si_x$ monokristalları əsasında radiasiyayadavamlı tenzoçevirici hazırlanmasına imkan verir ki, o da texnikanın müxtəlif sahələrində ölçmə proseslərinin avtomatlaşdırılmasına şərait yaradır.

М.К. Керимов, Ш.М. Аббасов, Ш.И. Аббасов.

РАДИАЦИОННО-СТОЙКИЕ ЭЛЕКТРОМЕХАНИЧЕСКИЕ ПРЕОБРАЗОВАТЕЛИ НА ОСНОВЕ НИТЕВИДНЫХ МОНОКРИСТАЛЛОВ Ge_{1-X} Si_X.

Исследования электромеханических характеристик нитевидных кристаллов $Ge_{1-x}Si_x$, подвергнутых электронному и γ облучению (Co^{60}), показали их повышенную радиационную стойкость по сравнению с другими приборами.

Полученные результаты позволяют сделать вывод о перспективности использования преобразователей на базе нитевидных монокристаллов Ge_{1-x} Si_x для практического осуществления автоматизации процессов измерения в различных областях техники.

Received: 17.09.01

EXCITON-EXCITON INTERACTION IN GaSe CRYSTAL ELECTROLUMINESCENCE SPECTRUM

G.I. ABUTALYBOV, S.Z. DZHAFAROVA , N.A. RAGIMOVA
Institute of Physics of the Azerbaijan National Academy of Sciences
H. Javid av. 33, Baku, 370143

Stimulated emission from the quasi-two-dimensional lamellar semiconductor GaSe was investigated under high electric fields and at the temperature 77 K. Increase of the polarized optical spectrum and quantum yield have been determined. Versus defects concentration and direction of the electric field applied to the specimens relative to optical C axis. The presence of three processes of intensification at the boundary of the fundamental absorption region, connected with mutual interaction of defects, free direct and non-direct excitons, has been confirmed.

INTRODUCTION

GaSe is a quasi-two-dimensional semiconductor with the indirect transition (space group $D_{3h}^{1} - \overline{p}6\,m2$) with the peak of the valence band in the G-point of the Brillouin zone and the bottom of the conduction band in M-point, i.e. two equivalent minima are situated on second order axes [1-5]. Moreover, an additional subband with the upward energy shift of 40 meV exists in the G-point. Fundamental direct and indirect transitions at 77 K are E_g^{dir}=2.177eV and E_g^{ind}=2.065eV, respectively. Binding energies of corresponding excitons are E^{dir}=20 meV and E^{ind}=43 meV [6-8]. Due to crystal structure, this free exciton becomes the resonance state (Philips, [9]) with the continuum of free electron states of indirect conduction band botton. Meanwhile impurities and phonon scattering might provide strong binding of these two types of state.

Large oscillator strength of the direct free exciton transition can provide free excitons recombination at energy substantially higher than E^{ind}. These processes become more probable at sufficiently high temperatures for electronic jumps to free exciton levels and will be maintained by high excitation density.

Results of investigations of stimulated emission in GaSe [10] with various intensities of the electric field applied along and normally to layers at T=77 K are given in the present paper. Three different lines of the stimulated emission in the region of direct and indirect excitons were observed.

In accordance with works [11-13] process of exciton-exciton interaction causes presence of the emission line shifted from the free exciton line to the region close to the bound exciton energy. Thus, mechanisms of optical spectrum intensification, which are responsible for observed lines, could be associated with joint exciton processes.

EXPERIMENTAL

Crystals were grown by Bridgman-Stockbarge method.

Experiments were carried out on monocrystalline plates of p-GaSe with mobility of holes and electrons 30÷40 and 150÷180 $cm^2/V{\cdot}s$ respectively at the room temperature. Specimens with dimensions 3x5x0.1 mm^3, specific resistance $10^5 \div 10^6$-Ω·cm at 300 K, obtained by simple cleaving along the cleavage plane, were used. Contacts were placed on the fresh-cleaved surface. In-Ga eutectic mixture was used as the electrode. Intercontact distance was 0.1-0.2 mm. The electrod-crystal contact processes have been excluded by measurement of all investigated volt-ampere characteristics at two opposite voltage directions. Crystals were cooled by direct immersion into the liquid nitrogen. Excitation was accomplished by the alternating voltage with the frequency 50 Hz. Electroluminescence was registered in two directions: from the surface normal to $\bar{C}$ axis and from the layer plane, containing $\bar{C}$ axis. Obtained spectra were analyzed by the DFC-24 spectrometer.

RESULTS

Electroluminescence spectra of available GaSe crystals in the region of the fundamental absorption edge can be combined into 4 groups. In accordance with X-ray analysis data, the ε-polytype is prevalent in specimens of No.1 type in comparison with other modifications; respectively crystals of this group are more perfect [14]. It could be seen from fig.1 that different distribution of lines intensities is observed for different groups of specimens: A–595 nm, B–615 nm, C–667 nm, D–688 nm. Short-wavelength line A having the same energy as line observed in the transmission spectrum and induced by free electron – hole pairs formation, can be ascribed to recombination of a direct free exciton. Strong resonance line of A exciton in specimens of No.1 type confirms that they are more perfect in comparison with specimens of other groups. Thus, for complex investigations of electroluminescence spectra, crystals of No.1 type with clearly defined exciton luminescence, have been chosen.

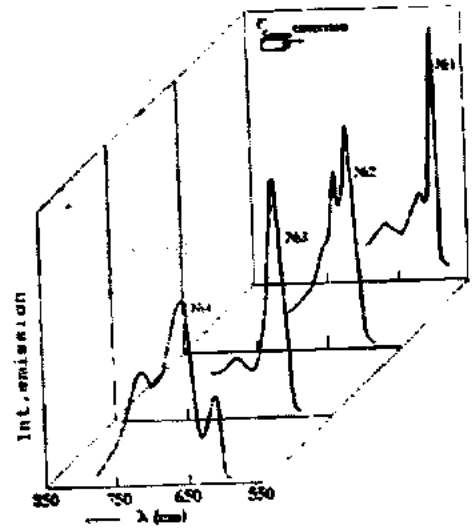

Fig.1. Electroluminescence spectra for various specimens of GaSe at 77 K

Figures 2, 3 demonstrate series of electroluminescence spectra obtained for GaSe at 77 K in emission directions $\bar{q} \perp \bar{C}$ and $\bar{q} \| \bar{C}$ respectively, with increase of the electric field intensity. Enlarged exciton electroluminescence spectrum at various intensities of the applied electric field ($\bar{q} \| \bar{C}$) is given in fig.4. Dependence of the energy position and relative intensity (E) are given in inset to fig.4. This dependence is represented by intersection of two curves in the region close to E=450 V/cm; they reflect two mutually incompatible phenomena: at E<450 V/cm lines are continuously shifting towards the low energy region, and beginning from E>450 V/cm, steep rise in intensity is observed which excludes longwavelength shifts.

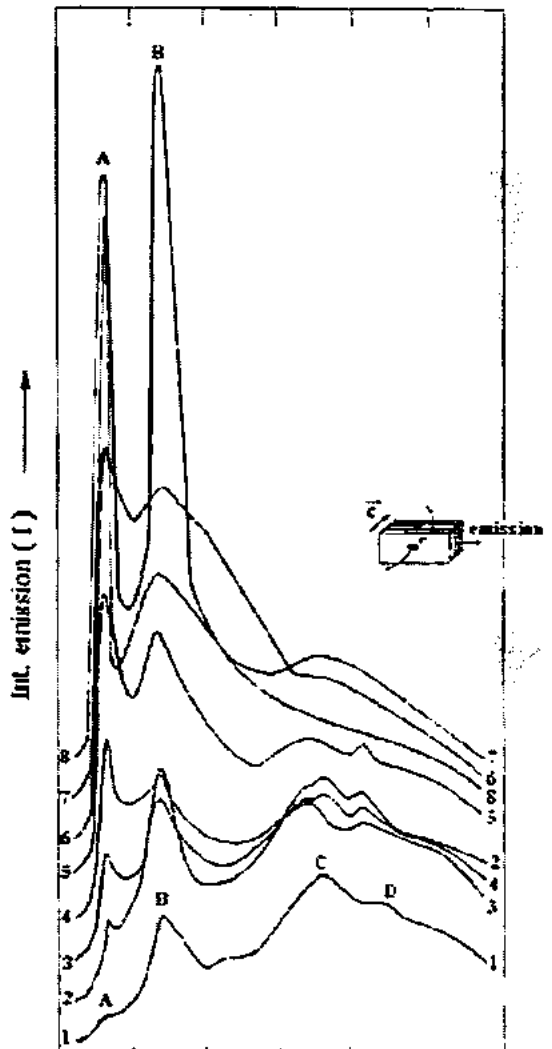

Fig. 2. Electroluminescence spectra for various specimens of GaSe (type No.1) in different fields, geometry q⊥C at 77 K 1-450; 2-530; 3-550; 4-660; 5-720; 6-760; 7-820; 8-840V/cm

With increase of E at $\bar{q} \| \bar{C}$ both A and B lines of a free exciton move to longwavelength region and have asymmetrical form with the low-energy tail. Meanwhile, C and D-lines demonstrate shortwavelength shifts. In case of $\bar{q} \perp \bar{C}$ geometry there is no energetic shift of lines.

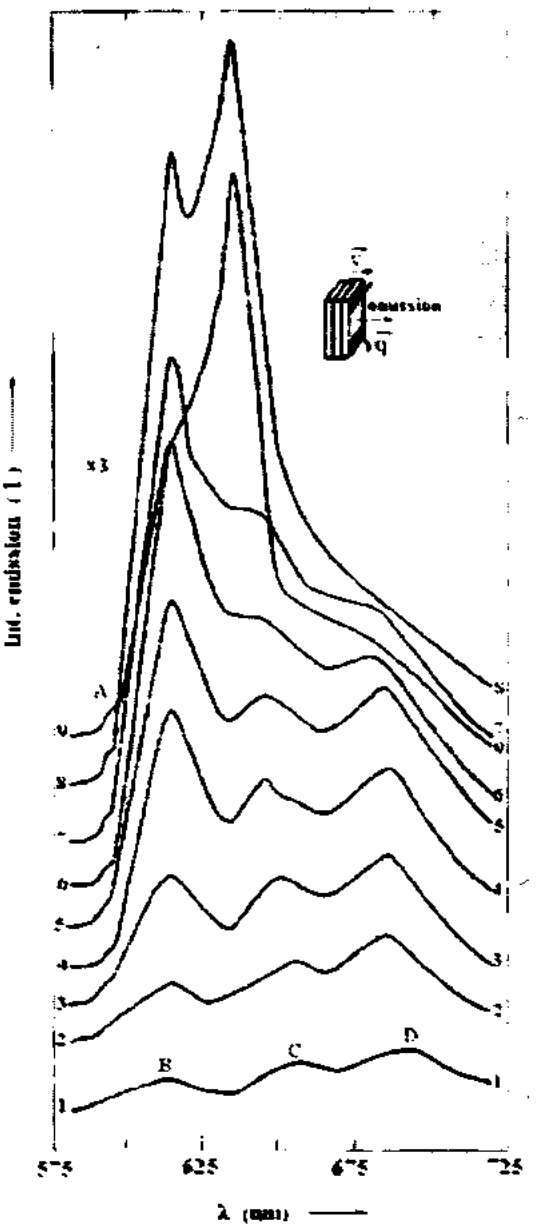

Fig. 3. Electroluminescence spectra for various specimens of GaSe (type No.1) in different fields, geometry q‖C at 77 K 1-230; 2-280; 3-340; 4-390; 5-450; 6-500; 7-560; 8-670; 9-780 V/cm

Alongside with increase of E up to the certain critical value E^{cr} in both observation directions, absolute value of the emission intensity rises. It is always higher in $\bar{q} \perp \bar{C}$ direction than in case of $\bar{q} \| \bar{C}$. Rise of the value E leads also to decrease of A and B lines half-widths in geometry $\bar{q} \perp \bar{C}$ (B and C in case of $\bar{q} \| \bar{C}$). Line A (B) is narrower in comparison with B (C). This shows that emission mechanism connected with A (B) is more favourable at higher intensities of electric fields. It is confirmed by the spectrum at E=760V/cm (580V/cm) for geometry $q \perp C$ ($q \| C$) where A (B) line dominates.

DISCUSSION

For the A-line the observed superlinear dependence on E excludes an impurity emission radiative recombination of the

bound exciton and phonon replica of the free exciton. Superlinearity, narrowing at E=720 V/cm $\vec{q} \perp \vec{C}$ with geometry (at E=450V/cm $-\vec{q} \| \vec{C}$), polarization and direction for the A-line emission allows to reveal stimulated emission in the course of annihilation of free direct excitons due to exciton-exciton interaction. Moreover the A-peak is badly observed in case of $\vec{q} \| \vec{C}$ geometry because reabsorption effect is strong when the light passes through the specimen and the low-energy tail of B-line is observed as the wide band with the peak of 2.015eV. It has been suggested [15] that B-line is a result of impurity-impurity emitting transition; authors [16] consider this line as phonon replica of the indirect bound exciton. However, further investigation [17] did not confirm these suggestions.

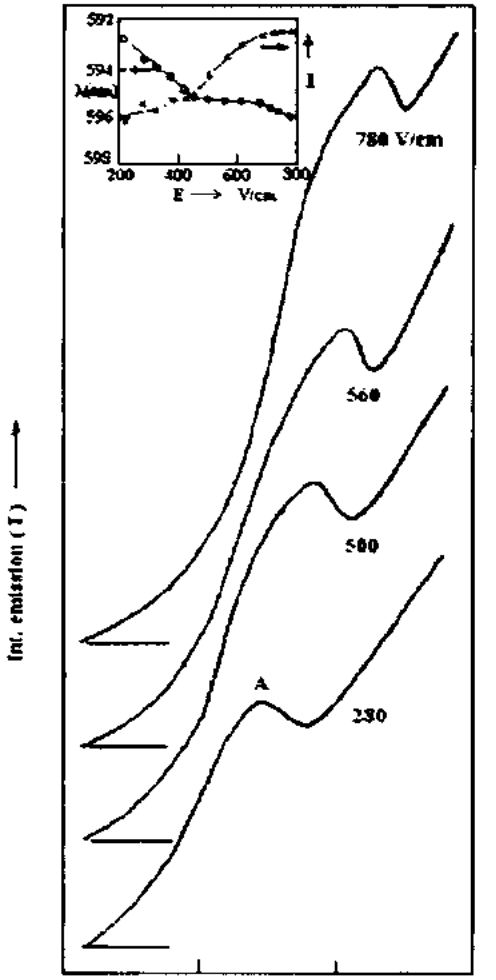

Fig.4. Exciton electroluminescence spectrum of GaSe specimen (type No.1) in different fields, geometry $q \| C$. Inset to Fig.4 is the dependence of energy position and relative intensity of A-line on E.

Polarization of B-line ($\vec{E} \| \vec{C}$) corresponds to indirect transition $M_3^+ - \Gamma_1^-$ allowed in GaSe that takes place with participation of the symmetry phonon M_1^- [18]. Magnitude of such phonon with dispersion contribution $\hbar\omega$=13meV [19]. Energy position $h\upsilon_e$=2.015eV of line satisfies to equation $h\upsilon_B = E_{g.exc.}^{ind} - \hbar\omega$, where $E_{g.exc.}^{ind}$=2.028eV is the value of indirect exciton zone in GaSe which is in good agreement with works [6-8], with the accuracy within several meV.

In our opinion the B-line is a result of stimulated emitting annihilation of free indirect excitons occurring at low temperatures with phonon emission. Important factor in favour of its exciton nature is coincidence of this line position in the luminescence spectrum with the energy position in the line caused by emitting decay of free indirect excitons.

It is difficult to understand the nature of the process responsible for the C-line. Indeed reliable data for a binding energy of indirect free exciton and for effective masses bound with M minimum of the conduction band are not given in literature. Nevertheless, we can observe that the functional dependence I_c on E is similar to the dependence of I_e vs E but it has different threshold voltage value. Larger halfwidth of C-line (52meV) can be ascribed to band-impurity emitting transitions in the energy region E>1.86eV. However, short-wavelength shift with E rising up to E_{thr} for indirect free exciton, superlinear dependence and narrowing beginning from $E > E_{thr}$ allow to assume that C-line is linked respectively by recombination through donor-acceptor pairs [20] and by exciton-exciton interaction (indirect excitons).

On the contrary, there might be no D-line due to joint exciton processes remoteness from exciton transition region and absence of stimulation even at high E values. Short wavelength shift with rise of E and long-wavelength shift with increase of time delay of registration relative to initiating pulse show that most probable mechanism stipulating this band must be recombination through donor-acceptor pairs.

Thus, in the region of the fundamental absorption edge of GaSe at 77 K we discovered three stimulated emission channels with $\vec{q} \perp \vec{C}$ ($\vec{q} \| \vec{C}$) geometry respectively working at various intensities of the applied electric field. In other words there are three mechanisms of inverse population with different threshold voltage in GaSe.

It should be noted that intensification of the optical spectrum and strong quantum yield of various optical intensification processes were registered which confirm the importance of GaSe material as the coherent light source. These results allow to suggest various methods of laser application in lamellar compounds.

[1] *R.W.G. Wyckopf*. Crystal Structures Interscience. N.Y., 1964, p. 587.

[2] *A.Kuhn, A.Chevy, R.Chevalier*. Phys.St.Sol. (a), 1975, 31, 2, p. 469.

[3] *F.Bassani, G.Pastori-Parravicini*. Nuovo Cim., 1967, B50, p. 95.

[4] *H.Kamimura, K.Nakao*. J.Phys.Soc.Japan, 1968, 24, p. 1313.

[5] *Von N.Schlutter* Helv. Phys. Acta, 1972, 45, 73. *E.Mooser, M.Schlutter* Proc.Int.Conf. on the Phys. of Semicond., 1972, p.750, Waszawa.

[6] *A.Cingolani, M.Ferrara and M.Lugara, F.Levy*. Phys. Rev., 1982, B 25, 2, p. 1174.

[7] *G.Belenki, V.Stopachinski*. Advances Phys. Sci., 1983, 140, 2, p. 233.

[8] *E.Aulich, J.L.Brebner, E.Mooser.* Phys.St.Sol., 1969, 31, p. 129.
[9] *J.C.Phillips.* Solid State Phys., 1966, 18, p. 56.
[10] *G.A.Akhundov.* Optics and Spectroscopy, 1965, 18, 4, p.743.
[11] *T.Ugumori, K.Masuda and S.Namba.* Phys.Lett., 1972, 38, 117, 2.
[12] *T.Ugumori, K.Masuda and S.Namba.* Solid State Communic., 1973, 12, 5, p.389.
[13] *L.N.Kurbatov, A.I.Dirochka, V.A.Sosin, B.B.Sinitsyn.* Phys.Stat.Solid. (USSR), 1977, 19, 3, p. 820.
[14] *H. Serizawa, Y.Sasaki, Y.Nishina.* J.Phys.Soc.Japan, 1980, 48, 2, p. 490.
[15] *J.P.Voitchovsky, A.Mercier.* Nuovo Cimento, 22B, 1974, p. 273.
[16] *N.Kuroda, Y.Nishina.* Phys.St.Sol. (a), 1975, 72, p. 81.
[17] *G.L.Belenki, M.O.Godzhaev, R.Kh.Nani, E.Yu.Salaev, R.A.Suleimanov.* Phys.Sol.Semicond. (USSR), 1977, 11, 5, p. 859.
[18] *M.Schluter.* Nuovo Cimento, 1973, 13B, 2, p. 313.
[19] *A.Mercier, J.P.Voitchovsky.* J.Phys.Chem.Sol., 1975, 36, p. 1411.
[20] *E.Zaks, A.Galperin.* USSR Academy of Sciences Izvestiya, Ser. Phys., 1973, 37, 3, 551.

H.İ. Abutahbov, S.Z. Cəfərova, N.A. Rəhimova

GaSe-NİN ELEKTROLÜMİNESSENSİYA SPEKTRİNDƏ EKSİTON-EKSİTON QARŞILIQLI TƏSİRİ

77K temperaturunda və elektrik sahəsinin yüksək qiymətlərində kvaziikiölçülü laylı yarımkeçiricinin stimullaşmış şüalanması öyrənilmişdir.

Defektlərin konsentrasiyası və nümunəyə tətbiq olunan elektrik sahəsinin optik ox $\vec{C}$ ilə təşkil etdiyi istiqamətdən asılı olaraq polyarizə olunmuş optik spektrin və kvant çıxımının güclənməsi ilə əlaqədar ölçmələr aparılmışdır.

Sübut olunmuşdur ki, fundamental udulma sərhədinin formalaşmasında iki proses-qarşılıqlı təsirdə olan defektlər və sərbəst düz və çəp eksitonlar iştirak edir.

Г.И. Абуталыбов, С.З. Джафарова, Н.А. Рагимова

ЭКСИТОН-ЭКСИТОННОЕ ВЗАИМОДЕЙСТВИЕ В СПЕКТРЕ ЭЛЕКТРОЛЮМИНЕСЦЕНЦИИ КРИСТАЛЛА GaSe

Стимулированное излучение от квазидвумерного слоистого полупроводника при высоких значениях электрического поля изучено при температуре 77 К. В зависимости от концентрации дефектов и направления прикладываемого к образцам электрического поля относительно оптической оси С, осуществлены измерения по усилению поляризованного оптического спектра и квантового выхода. Доказано наличие трех процессов усиления в области края фундаментального поглощения, связанного с совместными взаимодействиями дефектов, свободных прямых и непрямых экситонов.

Received: 12.02.02

THE ROLE OF DEFECTS IN SCATTERING OF PHONONS IN THE A^3B^5 ALLOYS

M.I. ALIYEV, R.N. RAHIMOV, D.H. ARASLY, A.A. KHALILOVA
Institute of Physics of the Azerbaijan National Academy of Sciences
H. Javid av. 33, Baku, 370143

On the base of thermal conductivities investigations the nature of defects in solid solution of GaSb-Ga_2Te_3, InAs-GaAs was analyzed in area 80-300K. It is shown that, the heat is transporting by phonons in area 80-300K and the most probably centers of their scattering are cation vacancy and impurity-vacancy complexes.

The present work includes an information about the results of research of thermal conductivity (K) of solid solutions $In_{1-x}Ga_xAs$ ($0<x<0.08$) and $(GaSb)_{1-x}(Ga_2Te_3)_x$ ($0<x<0.05$) in temperature range of 80-300 K. Measurements were carried out by a method a stationary thermal flow.

The temperature dependencies of thermal conductivity ($K(T)$) of solid solutions under investigation are shown on the figures 1 and 2. As seen from figures the value of K is reduced with increase of the second component and its temperature dependence is weaken what is typical for alloys. In the temperature dependence of thermal conductivity the anomalous change was observed.

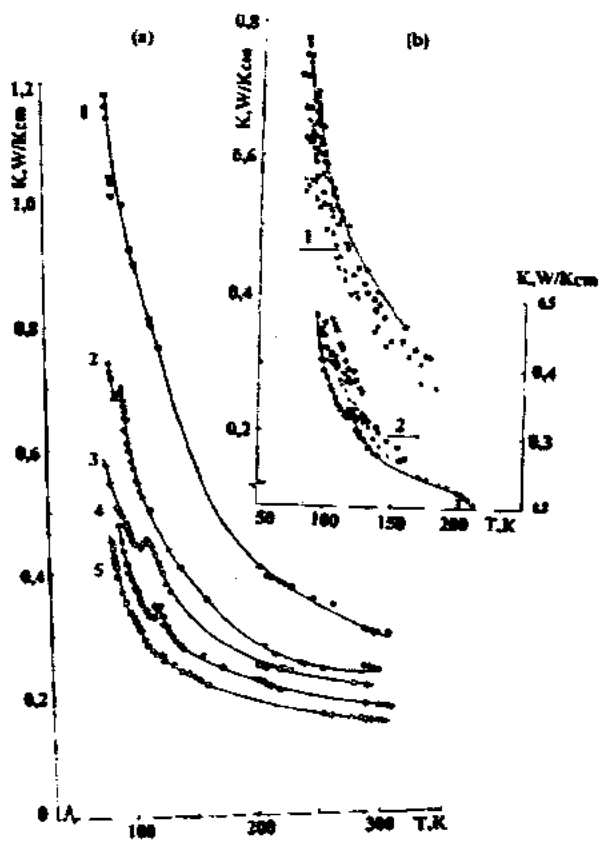

Fig.1. a) Thermal conductivity of $In_{1-x}Ga_xAs$ (x=0(1):0.1 (2): 0.02 (3): 0.04 (4): 0.08 (5) versus temperature.
b) Thermal conductivity of $In_{0.99}Ga_{0.01}As$ (1) and : $In_{0.96}Ga_{0.04}As$ (2); irradiated with electrons 6MeV energy and dose: ○ - F=0; ● - F=0.5·10^{17}e/cm^2; × - F=10^{17}e/cm^2; ∅ - F=1.5·10^{17}e/cm^2; Δ - F=2·10^{17}e/cm^2

So in $K(T)$ of $In_{0.99}Ga_{0.01}As$ within the narrow interval near T~ 90 K an obvious dip is observed. The decreasing depth of the dip in $K(T)$ and the shift of the temperature corresponding to this anomaly to the range of high temperatures are related with increase of the content of GaAs. In the case of GaSb-Ga_2Te_3 the second dip also appeared with increase of the content of telluride.

In the investigated range of temperatures the heat mainly is transported by phonons.

The electrons share of thermal conductivity counted in accordance with the Widemann-Franz formula is 2% of K_{exp}. Received results on the lattice thermal conductivity were analyzed by the Callaway model, by taking into account a probability scattering of phonons on phonons ($\tau^{-1}=B\omega^2T^4$) and on disorder alloy ($\tau^{-1}=A\omega^4$). In the case of GaSb-Ga_2Te_3 the scattering of phonons on the vacancy doping by Ga_2Te_3 has been taken into account too. The value of A calculated in accordance by the Klemens formula is differed of its storing value. It is need to take into account the phonons scattering on the other defects. It is possible, that these defects are the reason of the observed anomaly in $K(T)$. In the compounds of A^3B^5 (InSb, GaAs, GaSb) the dips were observed in $K(T)$ at 20-40K [1] and explained by the resonance acoustic phonons scattering. At present the nature of the centers of resonance scattering is not clear. The resonance phonons scattering is observed at comparatively "high" temperature in range 90-110 K in A^3B^5 alloys, in contrast with the binary compounds. We assume that a nature of this resonance center is related to complexes of impurity-vacancy. Our investigation of thermal conductivity of $In_{0.99}Ga_{0.01}As$ irradiated by electrons at 6 MeV energy and $2\cdot10^{17}$ e/cm^2 dose proved this assumption (fig.1b). As seen, the thermal conductivity decreases with a dose up to 10^{17}e/cm^2 and further increase of a dose leads to growth of K, moreover $K(T)$ becomes weaken with the dose. The dip in $K(T)$ becomes more expressive with the dose increase. The electrons part of thermal conductivity presents an insignificant part (2%) of K_{exp} [2], in spite of the fact that the electrons concentration, the electrical conductivity and the thermal power are changed with irradiation. Therefore all these changes of K with irradiation are connected with the scattering of phonons. The displacement of arsenic atom interassembly under the radiation leads to the formation of charged vacancy. The rate of migration of charged atoms and vacancies are different. Therefore along with the recombination the probability of their interaction with impurities and defects exists. The thermal conductivity with a dose is calculated in accordance with the Klemens formula [3], assuming that the concentration of vacancies is proportional to a dose of radiation:

$$K=K_L[1-(\omega_0/\omega_D)\,arctd\,(\omega_D/\omega_0)]\,.$$

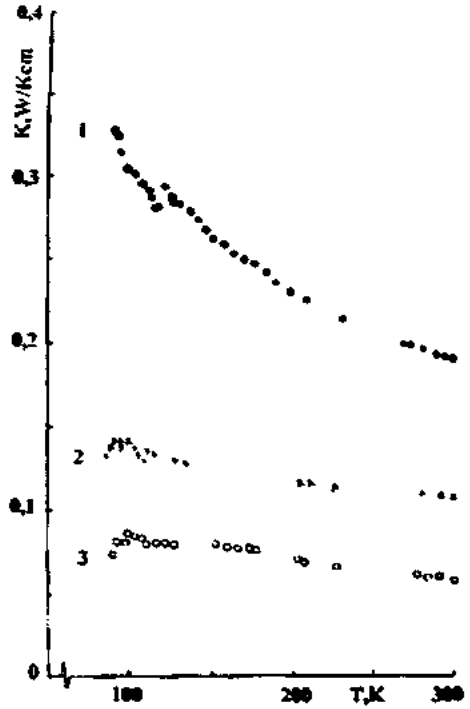

Fig.2. Thermal conductivity of $(GaSb_{3(1-x)}(Ga_2Te_3)_x$ (x=0.01 (1); 0.03 (2)

where $\omega_0^2/\omega_D^2=k_B/2\pi^2\ vK_L\omega_D A$, K_L is a lattice thermal conductivity, ω_D is a Debay frequency, v is a sound velocity.

In spite of fact that the change of thermal conductivity, conditioned by scattering of phonons on vacancies is more, than on arsenic atoms (at T=110K $F=10^{17}$e/cm^2, ΔK_0=0.024W/cmK and ΔK=0.05 w/cmK) their sum is almost twice less than results observed in experiment (ΔK). It means that at irradiation by fast electrons in InGaAs besides primary point defects the significant number of other defects probably complexes with vacancies participation arise. The role of complexes of impurity vacancy is evidently seen in $K(T)$ of solid solution of GaSb-Ga_2Te_3 (fig. 2). As known in this alloy by increase of telluride content the process of substitution of antimony by tellurium with the formation of cations vacancies and complexes occurs: vacancy – atom of Te and vacancy – 2 atoms of Te.

The existence of two dips in $K(T)$ probably indicatives to the scattering of phonons on both types of complexes.

[1] *N.K.S.Gaur, C.M.Bhandari, G.S.Verma* Physica 1966, №6, p.1048.

[2] *K.Guckelsberger and A.Brigss*. J.Phys.C. Solid State Phys. 1975, v. 8, L 195.

[3] *M.I.Aliyev, Kh.A.Khalilov, Sh.Sh.Rashidova*. DAN Azerb. 1988, т. 44, №7, p.31.

[4] *G.A.Ratsifaritana, P.G.Klemens*. Phonon scattering in condensed matter. New York. 1980.p.259-262.

M.İ. Əliyev, R.N. Rəhimov, D.H. Arash, A.Ə. Xəlilova

A^3B^5 ƏRİNTİLƏRİNDƏ DEFEKTLƏRİN FONON SƏPİLMƏLƏRİNDƏKİ ROLU

GaSb-Ga_2Te_3, InAs-GaAs bərk məhlulunda 80-300 K bölümündə istilikkeçiriciliyin tədqiqi ilə defeklərin təbiəti araşdırılmışdır. Göstərilən temperatur bölümündə istiliyin əsasən fononlarla daşınması və onların bərk məhluldakı kation tipli vakansiyalardan və aşqar-vakansiya komplekslərindən səpilməsinin üstünlük təşkil etdiyi göstərilmişdir.

М.И.Алиев, Р.Н.Рагимов, Д.Г.Араслы, А.А.Халилова

РОЛЬ ДЕФЕКТОВ В РАССЕЯНИИ ФОНОНОВ В СПЛАВАХ НА ОСНОВЕ A^3B^5

На основе исследований теплопроводности в интервале температур 80-300К проанализирована природа дефектов в твердых растворах GaSb-Ga_2Te_3 и InAs-GaAs. Показано, что в исследуемом интервале температур тепло в основном переносится фононами, и наиболее вероятными центрами их рассеяния являются катионные вакансии и примесь-вакансионные комплексы.

Received: 28.12.01

NON-MINIMAL INTERACTION AND SPECTRA OF IMPURITY STATES FOR LIGHT CARRIERS IN KANE'S SEMICONDUCTORS

A. M. BABAYEV
Institute of Physics of the Azerbaijan National Academy of Sciences
H. Javid av. 33, Baku, 370143

The energy spectrum of impurity states is calculated for Coulomb potential in Kane's type semiconductors using non-minimal interaction way.

The solutions of Dirac equations with minimal and non-minimal interactions terms were investigated in [1-4] by transforming relativistic equation into the Schrodinger like equation. It was shown [1] that if one makes a non-minimal replacement

$$\vec{p} \to \vec{p} - i\beta m\omega\vec{r} \tag{1}$$

in Dirac equation, where β is a diagonal matrix with elements ± 1, it can be transformed into the Schrodinger oscillator equation with parabolic potential and additional constant term the nature of which is connected with spin-orbital interaction.

It was shown in [5] that in the case of Kane's equation the non-minimal substitution of the form (1) also leads to the Schrodinger equation with harmonic oscillator potential. Other examples of non-minimal substitutions were considered in [6-7]. Non-minimal substitution of the form

$$\vec{p} \to \vec{p} - i\beta\frac{\vec{r}}{r} \tag{2}$$

in the Dirac equation leads to the Schrodinger equation with Coulomb potential. In this paper the same investigation was carried out for the Kane's equation describing the spectra of the electrons, light and heavy holes, and the spin-orbit splitting valence bands for the A^3B^5 type (InSb, InAs, GaAs and etc.) semiconductors. In the eight-band Kane's Hamiltonian the valence and conduction bands interaction are taken into account via the only matrix element P (so called Kane's parameter). The sistem of the Kane's equations including the nondispersional heavy holes band has a form [8-9]:

$$(\alpha \cdot k \cdot P + \beta \cdot G - E)\Psi = 0 \tag{3}$$

где

$$\alpha_x = \begin{pmatrix} 0 & 0 & \frac{-1}{\sqrt{2}} & 0 & \frac{1}{\sqrt{6}} & 0 & 0 & \frac{1}{\sqrt{3}} \\ 0 & 0 & 0 & \frac{-1}{\sqrt{6}} & 0 & \frac{1}{\sqrt{2}} & \frac{1}{\sqrt{3}} & 0 \\ \frac{-1}{\sqrt{2}} & 0 & 0 & 0 & 0 & 0 & 0 & 0 \\ 0 & \frac{-1}{\sqrt{6}} & 0 & 0 & 0 & 0 & 0 & 0 \\ \frac{1}{\sqrt{6}} & 0 & 0 & 0 & 0 & 0 & 0 & 0 \\ 0 & \frac{1}{\sqrt{2}} & 0 & 0 & 0 & 0 & 0 & 0 \\ 0 & \frac{1}{\sqrt{3}} & 0 & 0 & 0 & 0 & 0 & 0 \\ \frac{1}{\sqrt{3}} & 0 & 0 & 0 & 0 & 0 & 0 & 0 \end{pmatrix} \tag{4}$$

$$\alpha_y = \begin{pmatrix} 0 & 0 & \frac{i}{\sqrt{2}} & 0 & \frac{i}{\sqrt{6}} & 0 & 0 & \frac{i}{\sqrt{3}} \\ 0 & 0 & 0 & \frac{i}{\sqrt{6}} & 0 & \frac{i}{\sqrt{2}} & \frac{-i}{\sqrt{3}} & 0 \\ \frac{-i}{\sqrt{2}} & 0 & 0 & 0 & 0 & 0 & 0 & 0 \\ 0 & \frac{-i}{\sqrt{6}} & 0 & 0 & 0 & 0 & 0 & 0 \\ \frac{-i}{\sqrt{6}} & 0 & 0 & 0 & 0 & 0 & 0 & 0 \\ 0 & \frac{-i}{\sqrt{2}} & 0 & 0 & 0 & 0 & 0 & 0 \\ 0 & \frac{i}{\sqrt{3}} & 0 & 0 & 0 & 0 & 0 & 0 \\ \frac{-i}{\sqrt{3}} & 0 & 0 & 0 & 0 & 0 & 0 & 0 \end{pmatrix} \tag{5}$$

$$\alpha_z = \begin{pmatrix} 0 & 0 & 0 & \sqrt{\frac{2}{3}} & 0 & 0 & \sqrt{\frac{1}{3}} & 0 \\ 0 & 0 & 0 & 0 & \sqrt{\frac{2}{3}} & 0 & 0 & -\sqrt{\frac{1}{3}} \\ 0 & 0 & 0 & 0 & 0 & 0 & 0 & 0 \\ \sqrt{\frac{2}{3}} & 0 & 0 & 0 & 0 & 0 & 0 & 0 \\ 0 & \sqrt{\frac{2}{3}} & 0 & 0 & 0 & 0 & 0 & 0 \\ 0 & 0 & 0 & 0 & 0 & 0 & 0 & 0 \\ \sqrt{\frac{1}{3}} & 0 & 0 & 0 & 0 & 0 & 0 & 0 \\ 0 & -\sqrt{\frac{1}{3}} & 0 & 0 & 0 & 0 & 0 & 0 \end{pmatrix} \tag{6}$$

$$G = \begin{pmatrix} E_g & 0 & 0 & 0 & 0 & 0 & 0 & 0 \\ 0 & E_g & 0 & 0 & 0 & 0 & 0 & 0 \\ 0 & 0 & 0 & 0 & 0 & 0 & 0 & 0 \\ 0 & 0 & 0 & 0 & 0 & 0 & 0 & 0 \\ 0 & 0 & 0 & 0 & 0 & 0 & 0 & 0 \\ 0 & 0 & 0 & 0 & 0 & 0 & 0 & 0 \\ 0 & 0 & 0 & 0 & 0 & 0 & E_g + \Delta & 0 \\ 0 & 0 & 0 & 0 & 0 & 0 & 0 & E_g + \Delta \end{pmatrix} \tag{7}$$

$$\beta = \begin{pmatrix} 1 & 0 & 0 & 0 & 0 & 0 & 0 & 0 \\ 0 & 1 & 0 & 0 & 0 & 0 & 0 & 0 \\ 0 & 0 & -1 & 0 & 0 & 0 & 0 & 0 \\ 0 & 0 & 0 & -1 & 0 & 0 & 0 & 0 \\ 0 & 0 & 0 & 0 & -1 & 0 & 0 & 0 \\ 0 & 0 & 0 & 0 & 0 & -1 & 0 & 0 \\ 0 & 0 & 0 & 0 & 0 & 0 & -1 & 0 \\ 0 & 0 & 0 & 0 & 0 & 0 & 0 & -1 \end{pmatrix} \quad (8).$$

$$\Psi = \begin{pmatrix} \Psi_1 \\ \Psi_2 \\ \Psi_3 \\ \Psi_4 \\ \Psi_5 \\ \Psi_6 \\ \Psi_7 \\ \Psi_8 \end{pmatrix} \quad (9)$$

E_g is a band gap energy, Δ is a value of spin-orbital splitting and

$$k = -i\nabla \quad (10)$$

We substitute

$$\vec{k} \to \vec{k} - i\lambda\beta\frac{\vec{r}}{r}, \quad (11)$$

in Kane's system of equations. Expressing all components of the wave function by the first two we obtain:

$$\left(A - \frac{B}{r\hbar}L_z\right)\Psi_1 - \frac{B}{r\hbar}L_+\Psi_2 = 0 \quad (12)$$

$$\left(A + \frac{B}{r\hbar}L_z\right)\Psi_2 - \frac{B}{r\hbar}L_-\Psi_1 = 0 \quad (13)$$

где

$$A = E_g - E + \frac{P^2(3E+2\Delta)}{3(\Delta+E)E}(-\nabla^2 + \lambda^2 + \frac{2\lambda}{r}),$$

$$B = \frac{2}{3}\frac{P^2\Delta\lambda}{E(\Delta+E)} \quad (14)$$

$$L_\pm = L_x \pm iL_y,$$

L_x, L_y, L_z are angular momentum operator components. The spherical symmetry of this problem gives the possibility to express the solution of the differential equation in the form $F(r)Y(\theta, \varphi)$. Acting on the equation (13) with an operator L_- and using the commutative relations for operators $L_\pm$, L_z we obtain the expressions for $L_-\psi_2$. The substitution of the obtained value for $L_-\psi_2$ into the equation (12) gives two equations for $F(r)$:

$$\left(A - \frac{B}{2r} \mp \frac{B}{r}(l+\frac{1}{2})\right)F(r) = 0 \quad (15)$$

After substituti on of the values of A and B from (14) the equation (15) can be rewritten in the form:

$$\left(\frac{d^2}{dr^2} + \frac{2}{r}\frac{d}{dr} - \frac{l(l+1)}{r^2} + \frac{2m_n}{\hbar^2}\left(E' + \frac{N}{r}\right)\right)F(r) = 0 \quad (16)$$

where

$$E' = \frac{E(E-E_g)(E+\Delta)}{3E+2\Delta}\cdot\frac{3}{P^2}\frac{\hbar^2}{2m_n} - \frac{\hbar^2\lambda^2}{2m_n} \quad (17)$$

$$N = -\frac{\hbar^2\lambda}{m_n}\left(1 - \frac{\Delta}{3E+2\Delta}\left(\frac{1}{2} \pm (l+\frac{1}{2})\right)\right) \quad (18)$$

The solution of (16) reads [13]:

$$F(\rho) = \rho^l \exp(-\frac{\rho}{2})F(-n+l+1; 2l+2; \rho), \quad (19)$$

$F(-n+l+1, 2l+2, \rho)$ is a confluent hypergeometric function, $n-l-1=p$ must be positive integer or zero and

$$\rho = \frac{2}{\hbar}\sqrt{-\frac{2m_nE'}{\hbar}}r \quad (20)$$

The energy spectrum is determined by an expression:

$$E' = -\frac{N^2}{2\hbar^2}\frac{m_n}{n^2} \quad (21)$$

The Kane's parameter P is connected with effective mass m_n in a usual way:

$$P^2 = \frac{3\hbar^2}{2m_n}\frac{E_g(E_g+\Delta)}{3E_g+2\Delta} \quad (22)$$

Substituting the values of E', N, and P consequently from equations (17), (18) and (22) into (21) one can obtain the equation:

$$\frac{E(E-E_g)(E+\Delta)}{3E+2\Delta}\cdot\frac{3E_g+2\Delta}{E_g(E_g+\Delta)} - \frac{\hbar^2\lambda^2}{2m_n} = -\frac{\hbar^2\lambda^2}{2m_nn^2}\left(1 - \frac{\Delta}{3E+2\Delta}\left(\frac{1}{2} \pm \left(1+\frac{1}{2}\right)\right)\right)^2\frac{1}{n^2} \quad (23)$$

It is seen from (23) that the energy of impurity states depends on two quantum numbers n and l. This means that the degeneration on quantum number l is removed. Let us consider two limiting cases.

The first, when spin-orbital splitting is small in comparison with the energy gap ($\Delta << E_g$), takes place in all GaAs type wide band semiconductors. Then the equation (23) can be reduced to the form:

$$\frac{E(E-E_g)}{E_g}=\frac{\hbar^2\lambda^2}{2m_n}\left(1-\frac{1}{n^2}\right) \qquad (24)$$

For shallow acceptor states ($E>0$, $E<<E_g$) it can be obtained from (24):

$$E=-\frac{\hbar^2\lambda^2}{2m_n}+\frac{\hbar^2\lambda^2}{2m_n}\frac{1}{n^2} \qquad (25)$$

It is seen from (25) that the impurity states is connected with light carriers and has hydrogen-like spectrum. If one choose the value of λ in (11) in the form $\lambda=\frac{Ze^2m_n}{\chi\hbar^2}$ where χ is the static dielectric constant of the medium and Ze is the charge of the center then the equation (25) turns into the solution of the Shrodinger equation with the Coulomb potential shifted by $(Z^2e^4m_n/2\chi^2\hbar^2)$. Further we shall not consider this constant term in (25).

The equation (24) takes into account the non parabolicity of light carriers spectra too.

The second, when spin-orbital splitting is strong ($\Delta>>E_g$), which takes place in InSb or InAs. In this case the equation (23) transforms in to the form:

$$\frac{E(E-E_g)}{E_g}=-\frac{Z^2e^4m_n}{2\chi^2\hbar^2}\left(1-\frac{1}{2}\left(\frac{1}{2}\pm\left(l+\frac{1}{2}\right)\right)\right)^2 \qquad (26)$$

It is easy to obtain from (26) for the acceptor states ($E>0$, $E<<E_g$):

$$E_{\mp}=\frac{Z^2e^4m_n}{2\chi^2\hbar^2}\frac{(3\mp(2l+1))^2}{16}\frac{1}{n^2} \qquad (27)$$

The ground state energy ($n=1$, $l=0$) reads:

$$E_+=\frac{Z^2e^4m_n}{2\chi^2\hbar^2} \qquad (28)$$

Spectrum of donor states, which are placed below the E_g, can be obtained by the same way.

The problem of impurity states in Kane's type semiconductors, when Coulomb potential have been introduced into the Shroedinger equation by a standard way through the scalar potential was considered in [10-12]. As it was shown in these works there are two types of acceptor states in GaAs type crystals, connected with the valence bands. The first type states are connected with the heavy holes zone and described by the hydrogen-like spectrum. The second type states are due to the zone of light carriers and are described by the Dirac type spectrum. In InSb-type crystals the impurity states always are of Dirac-type.

We have shown in this paper that if one introduces Coulomb potential by non-minimal way then in Kane's model two types of solution are obtained depending on the value of spin orbital-splitting. For $E<<E_g$ we have the usual hydrogen like spectrum as for donor and as for acceptor states, the last being connected with the zone of light holes only. In the case when ($\Delta>>E_g$ the degeneration in orbital quantum number l is removed. However, in both cases the ground state energy have the form corresponding to the solution of the standard Shrodinger equation with Coulomb potential. This result is in accordance with the obtained earlier solutions for Kane's Hamiltonian which describes the spectrum of light charged carriers [10,11].

The author thanks F.M. Gashimzade and O.Z. Alekperov, for the useful remarks and discussion of results and E.Djafarov for attraction of his attention to works [6,7].

[1] *M. Moshinsky and A. Szczepaniak.* J.Phys. A:Math.Gen., 1989, 22, L817.
[2] *P.A. Cook.* Lett. Nuovo Cimento, 1971, 1, 419.
[3] *O. Castanos, A. Frank, R. Lopez and L.F. Urritaia.* Phys. Rev. D 43, 1991, 544.
[4] *F. Dominguez-Adame and M.A. Gonzales.* Euro Phys. Lett., 1990, 13193.
[5] *F.M.Gashimzade, A.M. Babayev.* FTT 44, 2002, №1, 155.
[6] *G.Levai and A Del Sol Mesa.* J.Phys. A:Math.Gen., 1996, 29, 2827.
[7] *G. Levai and F.Cannata.* J.Phys. A:Math.Gen., 1999, 32, 3947.
[8] *B.M. Askerov.* Kinetisheskiye effecti v poluprovodnikakh, L., "Nauka", 970.
[9] *A.I. Anselm.* Vvedeniye v teoriyu poluprovodnikov M., "Nauka", 1978.
[10] *L.B. Keldish.* JETF , 1963, 45, 2, 364.
[11] *M.A. Mekhtiev, G.B. Ibragimov, M.H. Khatamov.* Solid. St. Commun. 1984, v. 52, №4, 385.
[12] *B.L. Gelmont, M.I. Dyakonov.* FTP, 1971, 5, 11, 2191.
[13] *L.D. Landau.* Kvantovaya mekhanika, "Nauka", 1989, 767.

A.M. Babayev

QEYRİ-MİNİMAL QARŞILIQLI TƏSİR VƏ KEYN TİPLİ YARIMKEÇİRİCİLƏRDƏ YÜNGÜL YÜKDAŞIYICILARIN AŞQAR HALLARININ ENERJİ SPEKTRLƏRİ

Keyn tipli yarımkeçiricilərdə Kulon potensialı üçün aşqar halların enerji spektrləri qeyri-minimal qarşılıqlı təsir metodu ilə hesablanmışdır.

A.M. Бабаев

НЕМИНИМАЛЬНОЕ ВЗАИМОДЕЙСТВИЕ И СПЕКТР ПРИМЕСНЫХ СОСТОЯНИЙ ЛЕГКИХ НОСИТЕЛЕЙ ЗАРЯДА В КЕЙНОВСКИХ ПОЛУПРОВОДНИКАХ

Методом неминимального взаимодействия рассчитан энергетический спектр примесных состояний, связанных с кулоновским потенциалом в кейновских полупроводниках.

Received: 10.12.02

CORRELATION EQUATIONS of IONIC HYDRATATION in IONIC GROUPS of s-,p-,d-ELEMENTS

M.M. ASADOV

Institute of Physics of the Azerbaijan National Academy of Sciences
H. Javid av. 33. Baku, 370143

A connection between thermodynamic parameters of dissolution of ions in a solution is considered. In four groups of ions with the same electronic configuration the equations of correlation between enthalpy hydratation and ionic radii of hydrated ions are received.

During dissolution of substances there is an interaction of the dissolved substances to solvent. The re ceived products during dissolution form solvates. If as solvent water is used hydrates are formed.

It is possible to present. that a connection in hydrates is carried out as a result of two connected interactions: a) an electrostatic interaction between polar molecules of substances: b) an interaction owing to occurrence of hydrogen connection. Hydrogen connection realized between two atoms also has donor-acceptor character. Depending on system under investigation an energy of a hydrogen connection is 8-40 kJ/mole.

Two uncoupled electrons and a polarity of water molecule play an important role during dissolution of substances in water. Molecules of water are represented by four poles of charges. These charges are placed on vertices of a tetrahedron: two positive and two negative. The hydrogen connection between molecules of water together with an electrostatic attraction of electric dipole moments define properties of water.

In ionic crystals connection is caused basically by electrostatic interaction of opposite charged ions. Ionic crystals being dissolved in water form electrostatic associates. Owing to dissolution of crystals at first there are a destruction of its crystal lattice and creations of ions. and then hydration of these ions takes place. At dissolution polar molecules of water can be considered as electric dipoles.

Dielectric permeability of water ε under standard conditions is high and equal to ε=78.47. Value of ε is higher only for several liquids, for example for cyanhydrogen acid. For temperature dependence of dielectric permeability of water proceeding from experimental data [1] we have received: ε=178.5-0.3 T. Here T=273-373 K. The coefficient of correlation ρ calculated by a method of least square. is equal to -0.9967.

Change of Gibbs energy of dissolution process is determined from the equation

$$\Delta G_{dis} = \Delta H_{dis} - T\Delta S_{dis} . \qquad (1)$$

where ΔH_{dis} and ΔS_{dis} are enthalpy and entropy of dissolution accordingly.

Value of ΔG_{dis} which characterizes a change connected with removal of an ion from vacuum and put in solvent. can be estimated from Born equation:

$$\Delta G_{dis} = -N_A \frac{(Z_i e)^2}{2r_i}\left(1-\frac{1}{\varepsilon}\right). \qquad (2)$$

where N_A is Avogadro number: $Z_i e$ is a charge of hydrated ion;
r_i is ionic radius; ε is dielectric permeability of solvent. In any environment $\varepsilon > 1$.

From (2) it follows. that $\Delta G_{dis} < 0$. Value of ΔG_{dis} should become more negative for ions with smaller radius and the big charge in solvents with higher dielectric permeability. Values of ΔG_{dis} received from equation (2) at 298 K are in the agreement with the experimental data.

Value of ΔH_{dis} of ionic compound can be determined as follows:

$$\Delta H_{dis} = \Delta H_{hydro} + \Delta U_{lat} . \qquad (3)$$

where ΔH_{hydro} is enthalpy of hydrated ion. ΔU_{lat} is energy of destruction of a crystal lattice of compound .Here $\Delta H_{hydro} < 0$; $\Delta U_{lat} > 0$.

Value of ΔH_{hydro} is determined by a change of heat at transition of one mole of ions from vacuum into water solution. From formula (3) a total value of ΔH_{hydro} of hydrated cations and anions in a solution can be determined. Hydration enthalpy of anions (cations) of binary compound is determined from experimental data for ΔH_{hydro} for cations (anions) of the same compound.

From (3) it follows. that for different compounds ΔH_{dis} can have various signs. Enthalpy of dissolution of ionic crystals in water at 298 K usually has a negative sign. For some crystals in water $\Delta H_{dis} > 0$. for example for $CaCl_2 \cdot 6H_2O$. NH_4Cl. NaCl. $Na_2SO_4 \cdot 10H_2O$ [2].

Value of hydrated ion depends on its charge and ionic radius. Cations are hydrated stronger. than anions of similar charge. It is caused by the fact that positive area of a water dipole is located in space less compactly. than negative area of a dipole.

Absolute values of ΔH_{hydro} of hydrated ions are increased according with increase of ions charge. In groups of ions with the same electronic configuration with increase of ion radius absolute value ΔH_{hydro} of this ion decreases.

Dependences such as $\Delta H_{hydro} = f(r, Å)$ for different groups of ions are processed by a method of least square. As the initial data we used ΔH_{hydro} /2/and ionic radii $r(Å)$ [2, 3] for the following groups of ions with the same electronic configuration:

Li^+, Na^+, K^+, Rb^+, Cs^+ (I); Be^{+2}, Mg^{2+}, Ca^{2+}, Sr^{2+}, Ba^{2+} (II);
Sc^{3+}, Y^{3+}, La^{3+}(III): F^-, Cl^-, Br^-, I^- (IV)

In the table the obtained equations of correlation $\Delta H_{hydro} = ar(Å) - b$ are given(where a and b are constants) for

the groups (I)-(IV) ions with the same electronic configuration. Dependences between the indicated parameters of hydrated ions received by a method of least square are characterized by high coefficients of linear correlation.

Table.

The correlation equations for number of ions with the same electronic configuration.

Number of Ions (I)-(IV)	Correlation equation ΔH_{hydr}/kJ mole) = a r(Å)-b	Coefficient of correlation ρ
Li^+, Na^+, K^+, Rb^+, Cs^+	249 r, -723	0.9869
Be^{2+}, Mg^{2+}, Ca^{2+}, Sr^{2+}, Ba^{2+}	1247 r, -3029	0.9778
Sc^{3+}, Y^{3+}, La^{3+}	1837 r, -5606	0.9936
F^-, Cl^-, Br^-, I^-	250 r, -784	0.9921

[1] *I.T.Goronovski, J.P. Nazarenko, E.F. Necratch.* Brief chemistry directory. Kiev. Naukova Dumka, 1974, p. 767.

[2] *M.H. Karapetiants, S.I. Drakin.* General and inorganic chemistry. M.Chemistry, 1981, p.158.

[3] *Ch. Kittel.* Introduction to Solid State Physics. Trans. from En. M.Science. 1978, p.144.

M.M. Əsədov

s-, p-, d- ELEMENTLƏRİ İONLARININ HİDRATLAŞMASININ KORRELYASİYA TƏNLİKLƏRİ

İonların su məhlulunda həll olması zamanı termokimyəvi parametrlər arasındakı əlaqələr araşdırılmışdır. Eyni tipli elektron konfiqurasiyasına malik olan s-, p-, d- elementləri ionları üçün korrelyasiyalar tapılmışdır. Dörd qrup ionlar üçün korrelyasiya tənlikləri alınmışdır. Hidratlaşma entalpiyası və hidratlaşan ionların radiusları arasında empirik asılılıqlar təyin edilmişdir.

М.М. Асадов

КОРРЕЛЯЦИОННЫЕ УРАВНЕНИЯ ГИДРАТАЦИИ В ПОДГРУППАХ ИОНОВ s-, p-, d- ЭЛЕМЕНТОВ

Рассмотрена связь между термодинамическими параметрами растворения ионов в растворе. В четырех подгруппах ионов s- , p- , d- элементов, с однотипной электронной конфигурацией методом наименьших квадратов получены уравнения корреляции. Установлена связь между энтальпией гидратации и ионными радиусами гидратируемых ионов.

Received: 25.01.02

THE STIMULATION OF MULTIPLICITY OF THE LIGHT TO DARK CURRENTS RATIO IN $PbGa_2Se_4$ SINGLE CRYSTAL

B.G. TAGIYEV, N.N. MUSAYEVA, R.B. JABBAROV
Institute of Physics of the Azerbaijan National Academy of Sciences
H. Javid av. 33, Baku, 370143

The volt-amperecharacteristic of $PbGa_2Se_4$ single crystals in the darkness and under the illumination 200 lx has been investigated in the broad interval of electric fields.

The stimulation of multiplicity the light to dark currents ratio at 200 lx has been revealed. It has been established that deep levels of the crystal are filled with the illumination increase, in the consequence of what the height maximum in dependences of the light to dark current ratio multiplicity on voltage ($k \sim U$) reduces.

The family of triple chalcogenide compounds, with the common formula $A^{II}B_2^{III}C_4^{VI}$ (where A-M, Pb; B-Ga, In; C-Se, S) belongs to the perspective semiconductive materials, which at present has studied in details in physics and technology of semiconductors.

Crystals on the base of above-mentioned compounds, possessing expressive photoconductive properties, are the perfect base for the creation of light-emitting and electro-photographic devices, solar elements and other converters.

$PbGa_2Se_4$ compound, belonging to this family, is photosensitive in the broad spectrum region (0.400÷1.200μm). Photoconductivity (PC) spectra at various applied electric fields, the temperature blacking of the photocurrent (TBP), PC kinetics and etc. [1] have been investigated in $PbGa_2Se_4$ crystals in works published earlier.

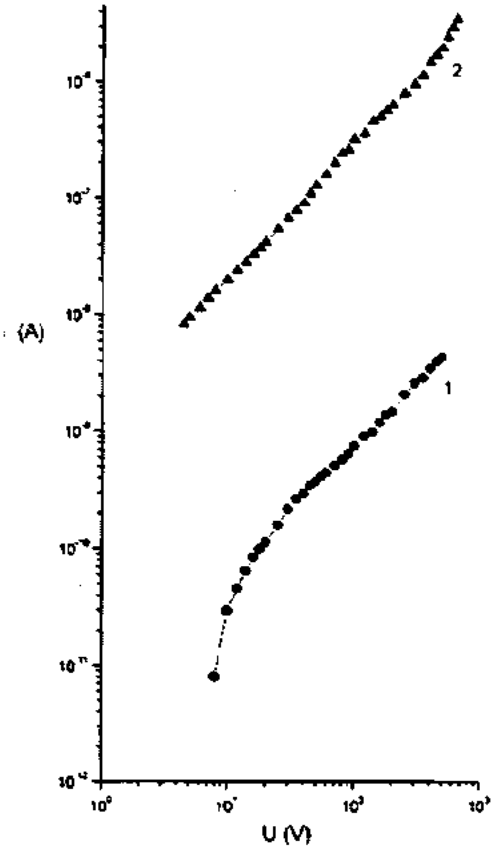

Fig.1. Volt-ampere characteristic of $PbGa_2Se_4$ single crystal in the darkness (1) and under the illumination 200 lx (2).

$PbGa_2Se_4$ single crystals, obtained by the Bridgman-Stockbarger method, are high-ohmic semiconductors ($\rho \sim 10^{10} \div 10^{11}$ ohm·cm). Direct and indirect optical transitions of E_{gi}=2.28eV and E_{gd} =2.35eV energies corresponding to 300 lx [2] have been revealed as a result of optic research in the interval of the photon energy 2.24÷2.46eV.

As it is known, the multiplicity of light to dark currents ratio is one of the main characteristics of photosensitive crystals. Authors of works [3-5] have worked out the theoretically based methods of experimental photocurrent curves analysis, based on approximations in the constant field regime.

Experimental research has been carried out on the device, assembled in monochromator MDR-12 base. Samples have been illuminated by the filament lamp.

Volt-ampere characteristics (VAC) of $PbGa_2Se_4$ in the darkness and by illuminations 200 lx are presented on fig.1. As it is seen from the fig., the dark current grows sharply in weak electric fields and the linear part is observed on VAC by the illumination at the same field values. The sharp increase of the dark current up to 10^{-10}A is connected with the contact surface barrier creation in the sample, included in the locking direction. The barrier breakdown in the consequence of the impact ionization in the volume charge region occurs as a result of the linear increase and electrons are injected into the space from the contact.

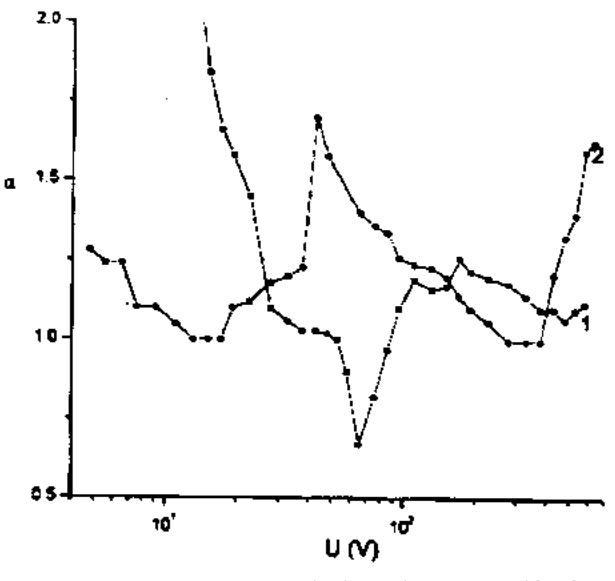

Fig.2. The dependence α on U in the darkness (1) and by the light 200 lx (2). (1) – n_{to} = 6·10⁶ cm⁻³ ; D_t^*=6·10⁻³ ; d_k= =1.1·10⁻⁷ cm; $\Delta\varepsilon$=0.78eV; $n_{t_{max}}$=2.6·10⁶ cm⁻³; (1)- n_{to} = =6·10⁶ cm⁻³ ; D_t^*=6·10⁻³ ; d_k= 1.1·10⁻⁷ cm; $\Delta\varepsilon$=0.78eV; $n_{t_{max}}$=2.6·10⁶cm⁻³; $I_{t_{max}}$=1.22·10⁻⁹A; ρ_k/e= 3.88·10¹¹cm⁻³; (2) - n_t=2.24·10⁶ cm⁻³.

The sublinear part with the degree value $0<\alpha_m<1$, which characterizes the constant field regime on the intercontact layer, is observed on the curve at the further voltage increase (fig.2, curve 1). Using the minimal value α_m =0.67, the initial contact concentration n_{k0}, the effective transparency of contact barrier D_k^*, contact barrier d_k width have been found [6,7]:

$$\Delta\varepsilon = kT\ln\frac{N_c}{n_{k0}} \qquad (1)$$

where

$$N_c = 2\left(\frac{2\pi m_n kT}{h^2}\right)^{3/2} \approx 10^{19}\,cm^{-3}\cdot\left(\frac{m_n}{m}\frac{T}{300K}\right)^{3/2}$$

is the effective density of states in the conduction band.

The minimum possible contact concentration and the current intensity determining the decay limits of the contact emission in the monopole injection regime, are calculated by formulae:

$$(n_k)_{min} = \left(2-\frac{\alpha_m}{1-\sqrt{1-\alpha_m}}\right)exp\left(\sqrt{1-\alpha_m}\right)\frac{I_m L}{e\mu S V_m} \qquad (2)$$

$$I_{min} = \left(2-\sqrt{1-\alpha_m}\right)exp\left(\sqrt{1-\alpha_m}\right)I_m \qquad (3)$$

A junction from the linear part to the sublinear allows to estimate the contact density of the spatial charge $|\rho_k|$:

$$|\rho_k| = \frac{\varepsilon V_j}{2\pi L^2} \qquad (4)$$

Here V_j is the initial value of the voltage of $\alpha(V)$ function decay point from the unit. The jump (α_{max}=1.7, U_{max}=42.5V, I_{max}=1·10^{-7}A), is observed on the light in dependences α~U (fig.2, curve 2); and current increase with the voltage occurs in strong fields. The maximal value α_{max} has allowed to determine some important crystal parameters [8], including anode concentration – n_k

$$nk = 2\frac{\alpha_m^2}{\alpha_m+1}\cdot\frac{I_m L}{e\mu V_m S} \qquad (5)$$

The stimulation character of the dependence of the light to dark currents ratio multiplicity on the applied voltage is perfectly illustrated on fig 3. The multiplicity reaches K_{max} =5·10^2 by the light 200 lx. Deep levels of the crystal are filled with the illumination increase and by this the maximum height decreases:

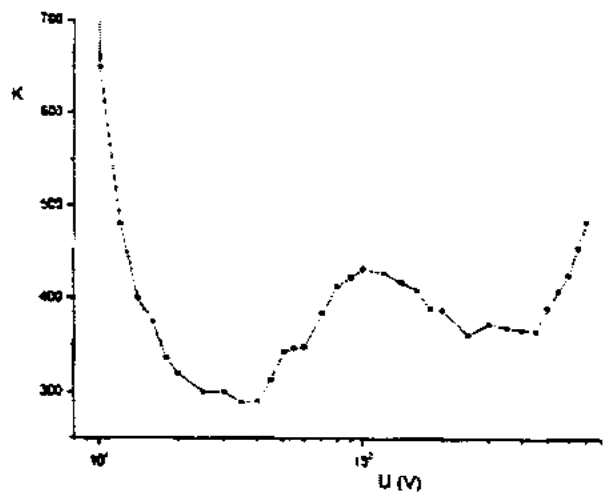

Fig.3 The dependence K on U.

[1] *B.G. Tagiyev, O.B. Tagiyev, R.B. Jabbarov, N.N. Musayeva.* Inorganic materials, 1999, v.36, №1, pp. 333-35.

[2] *B.G. Tagiyev, N.N. Musayeva, R.B. Jabbarov.* FTP, 1999, v.33, № 1, pp. 39-41.

[3] *A.N. Zyuganov, S.V. Svechnikov.* "Injection-contact phenomena in semiconductors", Kiev, Naukova Dumka, 1981.

[4] *Y.V. Costyukevich, S.V. Svechnikov, P.S. Smertenko.* Optoelectronics and semiconductive technique, 1993, issue 26, pp. 70-75.

[5] *A.N. Zyuganov, L.V. Zaryalova, A.M. Ivanov, S.V. Svechnikov, P.S. Smertenko.* Optoelectronics and semiconductive technique, 1989, issue 16, pp. 42-44.

[6] *Z.V. Berishvili, A.N. Zyuganov, S.V. Svechnikov, P.S. Smertenko.* Semiconductive technique and microelectronics, 1978, №28, pp.23-31.

[7] *A.N. Zyuganov, S.V. Svechnikv, A.Y. Tkhorik, Y.P. Shul'ga.* UPJ, 1997, № 1, pp. 370-375.

B.Q. Tağıyev, N.N. Musayeva, R.B. Cabbarov

PbGa$_2$Se$_4$ MONOKRİSTALLARINDA İŞIQ CƏRƏYANLARININ QARANLIQ CƏRƏYANA NİSBƏTƏN TƏRTİBİNİN STİMULLAŞMASI

PbGa$_2$Se$_4$ monokristallarının qaranlıqda və 200 lk işıqda və geniş elektrik sahə intervalında volt-amper xarakteristikaları tədqiq olunmuşdur.

İşiq cərəyanın qaranlıq cərəyana nisbətən tərtibinin stimulyasiyası 200 lk-da müşahidə olunmuşdur. Müəyyən olunmuşdur ki, işıqlanmanın artması ilə kristalın dərin səviyyələri dolur, nəticədə isə işıq cərəyanının qaranlıq cərəyana nisbətən tərtibinin gərginlikdən asılılığında (k~U) maksimumun hündürlüyü azalır.

THE STIMULATION OF MULTIPLICITY OF THE LIGHT TO DARK CURRENTS RATIO IN $PbGa_2Se_4$ SINGLE CRYSTAL

Б.Г. Тагиев, Н.Н. Мусаева, Р.Б. Джаббаров

СТИМУЛЯЦИЯ КРАТНОСТИ ОТНОШЕНИЯ СВЕТОВОГО ТОКА К ТЕМНОВОМУ В МОНОКРИСТАЛЛЕ $PbGa_2Se_4$

Исследована вольтамперная характеристика монокристаллов $PbGa_2Se_4$ в темноте при освещенности 200 лк в широком интервале электрических полей.

Обнаружена стимуляция кратности светового тока к темновому при 200 лк. Установлено, что с увеличением освещенности глубокие уровни кристалла заполняются, в результате чего уменьшается высота максимума на зависимости кратности отношения светового тока к темновому от напряжения ($k \sim U$).

Received:20.11.01

HEAT CAPACITY AND THERMODYNAMIC PROPERTIES OF $TlCoS_2$

M.A. ALJANOV, E.M. KERIMOVA, S.I. MEKHTIEVA,
M.D. NADJAFZADE, S.G. SULTANOV, G.M. AKHMEDOVA
Institute of Physics of the Azerbaijan National Academy of Sciences
H. Javid av. 33, Baku, 370143

This paper deals with the investigation of the heat capacity of the ferromagnetic compound $TlCoS_2$ in the temperature interval 55-300K. It is shown that behavior of the magnetic part of the heat capacity of $TlCoS_2$ is characteristic of for quasi -low -dimensional magnets. There have been calculated thermodynamic parameters of changes of $TlCoS_2$ entropy and enthalpy on the temperature dependence of the heat capacity.

In paper [1] there have been synthesized and investigated some physical properties: structure, magnetization and paramagnetic susceptibility of $TlCoS_2$ compound. It is shown that $TlCoS_2$ crystallizes as the hexagonal structure (c/a ≈6) and is the low-dimensional ferromagnetic with the Curie temperature 112K. Study of influence of space and spin anisotropy on the behavior of the magnetic heat capacity, and also on the behavior of the phase junction in the ordered state is of great interest.

In this paper we measure heat capacity of $TlCoS_2$ compound in the temperature interval 55-300K and calculate main thermodynamic parameters (change of entropy, enthalpy). Heat capacity is measured by the adiabatic method [2]. By measurement of the heat capacity there have been used samples, which were synthesized and studied in work [1].

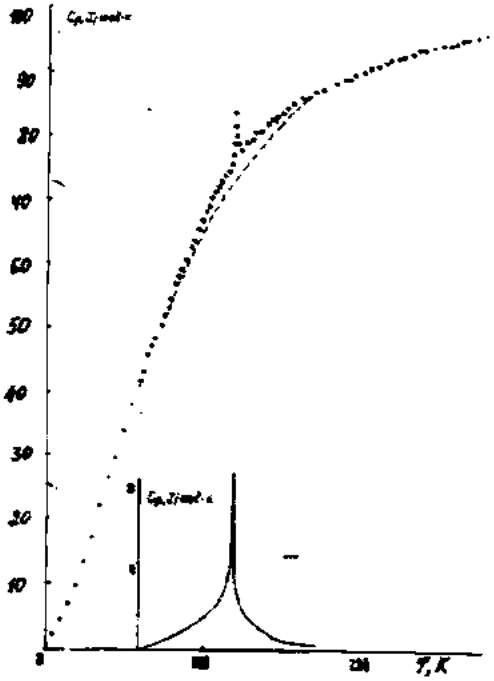

Fig.1. Temperature dependence of the heat capacity of TeCoS2: • - experimental points, x - calculated, — - lattice and ___ - magneto – parts of the heat capacity.

In fig.1 the temperature dependence of $TlCoS_2$ heat capacity is shown. As it is seen in the dependence $C_p(T)$ pronounced λ- anomaly has not been obseved. In the region of 118K there have been observed the minor anomaly, which apparently is connected with the magnetic junction. It was impossible to determine critical parameters of the magnetic phase junction because of the small anomaly. Temperature, corresponding to this anomaly is close to the temperature of the three-dimensional junction defined from the magnetization in work [1].

To isolate a magnetic contribution to a heat capacity of a magnetically ordered substance, as a rule one can choose such a nonmagnetic reference compound whose heat capacity and its temperature dependence are close to the lattice contribution to the heat capacity of an investigated magnetic substance. We could not find an isostructural diamagnetic compound for magnetic heat capacity liberation because of the deficiency of necessary data. Therefore we used $TlCrS_2$ compound, having the like structure with $TlCoS_2$. Temperature dependence of $TlCrS_2$ lattice heat capacity is described by V.V. Tarasova formula [3] with the Debye temperature θ_2 =342K and θ_3 =103K (data on $TlCrS_2$ heat capacity is in the press). We note, that in spite of Tarasov's model simplicity it is used for description of the lattice heat capacity of laminated and chain magnetic compounds with less number of adjustable parameters in the region $C_{lat} >> C_{mag}$. We used the method of corresponding states [4] with r =1.022 for calculation of C_{lat} of $TlCoS_2$ as compared with $TlCrS_2$. Obtained lattice (broken line) and magnetic (solid line) heat capacity ($C_{mag}=C_{ex}- C_{vib}$) of $TlCoS_2$ are presented in fig. 1. As it is seen, the magnetic heat capacity has wide maximum at $T_{c\ max}$=118K and approaches to zero above ~ 180K. The presence of wide maximum with high-temperature line on the curve $C_{mag}(T)$ above T_c is the characteristic feature of the magnetic $TlCoS_2$ heat capacity. Such behavior of the heat capacity is characteristic of quasi-two-dimensional systems. Below ~180K the compound $TlCoS_2$ apparently passes to the three- dimensional magnetic ordering connected with to distant orders, i.e. $TlCoS_2$ becomes the to three- dimensional magnetic. There have been observed the contribution of the close order to the heat capacity at higher temperature.

Magnetic energy and entropy, calculated with integration C_{mag} and C_{mag}/T are equal to ΔH_{mag}= 154.6 J/mol, ΔS_{mag}= 1.41 J/mol·K, respectively.

In paper [1] by investigation of magnetic properties and based on the laminated structure authors come to the conclusion that $TlCoS_2$ is the low- dimensional magnetic with the ferromagnetic ordering. Magnetic susceptibility of low- dimensional magnetics also has specific displays different from three - dimensional systems. Dependence $\chi(T)$ is described by Curie-Weis law in the range of high temperatures. With the decrease of the temperature $\chi(T)$ has the wide maximum connected with formation of the close order [5]. However such behavior of the susceptibility is not

observed for $TlCoS_2$ [1]. We note that using the Gudenaf model based on competition between direct cation-cation and indirect cation-anion exchanges, authors of paper [6] tried to explain the two-dimensional ferromagnetic behavior of the ordering in $TlCrS_2$. Complete structural data are necessary for application of the similar explanation in case of $TlCoS_2$.

On the base of the temperature dependence of the heat capacity there have been calculated thermodynamic functions (change of entropy and enthalpy of $TlCoS_2$) in the range 0-300K. Below ~ 55Kthe value $C_p(T)$ was calculated on the Debay law. Then the value of the Debay temperature was found on the experimental value of the temperature at ~ 60K.

Table presents values of $TlCoS_2$ entropy and enthalpy change.

T, K	50	100	150	200	250	300
S_T-S_0, *J molK*	28.82	62.58	94.88	120.0	140.6	157.9
H_T-H_0, *J mol*	0.748	3.354	7.240	11.60	16.23	21.01

[1] *R.Z.Sadikhov, E.M.Kerimova, Y.G. Asadov, R.K. Veliev.* FTT, 2000, V. 42, №8, pp. 1449-1450.

[2] *M.A. Aldjanov, N.G. Guseinov, G.D. Sultanov, M.D.Najafzade.* Phys. Stat. Sol. (b) 1990, v. 159, №2, p.107-110.

[3] *V.V. Tarasov.* Problems of glass physics. Moscow, Gosstroyizdat, 1979, p. 256.

[4] *R. Chisholm, J. Stout.* J. Chem. Phys., 1962, v.36, №2, pp. 972-979.

[5] *M. Steiner, J. Villain, C.G. Windsor.* Adv. Phys., 1976, v.25, №2, pp. 87-209.

[6] *M. Rosenberg, W. Knille.* J. Phys. Chem. Sol., 1982, v.43, №2, pp.87-95.

M.A. Alcanov, E.M. Kərimova, S.İ. Mehdiyeva, M.D. Nəcəfzadə, S.G. Sultanov, G.M. Əhmədova

$TlCoS_2$ -NİN İSTİLİK TUTUMU VƏ TERMODİNAMİK XASSƏLƏRİ

İşdə 55-300 intervalında $TlCoS_2$ ferromaqnit birləşməsinin istilik tutumu tədqiq edilmişdir. Göstərilmişdir ki, $TlCoS_2$-nin maqnit istilik tutumu kvaziaşağı ölçülü maqnetiklərə xas olan gedişə malikdir. İstilik tutumunun gedişinə əsasən $TlCoS_2$-nin termodinamik parametrləri entropiya və entalpiya hesablanmışdır.

М.А. Алджанов, Э.М. Керимова, С.И. Мехтиева, М.Д. Наджафзаде, С.Г. Султанов, Г.М. Ахмедова

ТЕПЛОЕМКОСТЬ И ТЕРМОДИНАМИЧЕСКИЕ СВОЙСТВА $TlCoS_2$

В работе исследована теплоемкость ферромагнитного соединения $TlCoS_2$ в интервале 55-300K. Показано, что поведение магнитной части теплоемкости $TlCoS_2$ характерно для квазинизкомерных магнетиков. На температурной зависимости теплоемкости вычислены термодинамические параметры изменения энтропии и энтальпии $TlCoS_2$.

Received: 12.02.02

PHOTO-, ROENTGEN-SENSITIVITY AND ROENTGENOAMPERE CHARACTERISTICS OF $TlInSe_2$- $TlSbSe_2$ SYSTEM SINGLE CRYSTALS

E.M. KERIMOVA, S.N. MUSTAFAEVA, S.I. MEKHTIEVA, FIRUZA M. HASHIMZADE

Institute of Physics of the Azerbaijan National Academy of Sciences
H. Javid av. 33, Baku, 370143

The influence of composition of $TlIn_{1-x}Sb_xSe_2$ solid solutions on photosensitivity and roentgendosimetric parameters was investigated. $TlIn_{0.999}Sb_{0.001}Se_2$ single crystals had the highest value of roentgen-sensitivity (K_σ): for example, at dose E=0.75 R/min and "effective hardness" U_a=25 keV K_σ was equal to 0.278 min/R.

The study of roentgen-ampere characteristics of $TlIn_{1-x}Sb_xSe_2$ single crystals showed that dependence of roentgen-current ($\Delta I_{E,0}$) on dose of x-ray (E) is as follows: $\Delta I_{E,0} \sim E^{\alpha}$. It was shown, that at In→Sb substitution the coefficient α increases. For example, in $TlIn_{0.999}Sb_{0.001}Se_2$ α=0.96÷0.46, but in $TlIn_{0.9955}Sb_{0.0045}Se_2$ α=1.70÷0.60 at U_a=25÷50 keV.

Obtained results show, that crystals of $TlInSe_2$- $TlSbSe_2$ system can be used for the production of roentgendetectors.

Search of new semiconductive materials is one of the cardinal problems of modern solid state physics and crystallochemistry. Revealing of new materials along with the extention of scientific knowledge opens the new prospects: as a rule new substances especially with chain-layered structure show new properties and promote to the solution of new technical problems.

Among chain-layered semiconductors of $A^3B^3C_2^6$ (*A*-Tl; *B*-In, Ga; C-S, Se, Te) the $TlInSe_2$ group is the most sensitive to visible and roentgen radiation. Their photoelectric and roentgendosimetric characteristics are described in [1-8].

In [1] there have been studied influence of Ag, Cu and Sn on photoelectric properties of $TlInSe_2$ single crystals. In [2,4,5] results of intercalation influence by Li ions on photo- and roentgen conductivity of $TlInSe_2$ have been presented.

The aim of present paper is to treat influence of partial substitution of In ions in $TlInSe_2$ by Sb ions on their photo- and roentgendosimetric parameters.

$TlSbSe_2$ wide-band crystals are differed by high photosensitivity and because of character of chemical bond due to pronounced lamination are rather interesting objects for study [9-13].

$TlInSe_2$ and $TlSbSe_2$ compounds are synthesized from initial materials of Tl-000; In-000; Sb-000; Se- 000 by direct component melting taken in stoichiometric relation in evacuated up to $1.3 \cdot 10^{-3}$ Pa and sealed quartz ampules. For $TlSbSe_2$ production we increase furnace temperature up to 878K and hold melt for 5-6 hours with continuous vibration and further slow cool it up to annealing temperature. As $TlSbSe_2$ compound undergoes structural phase transition at 653K it is annealed at 693K and 573K for 200 hours.

$TlInSe_2$-$TlSbSe_2$ cutting alloys are prepared from preliminary synthesized compounds $TlInSe_2$ and $TlSbSe_2$ by heating in evacuated ampules not above 1123K with the use of vibration mixing. Annealing is carried out at 693÷773K for 240 hours.

Obtained samples have been studied by differential-thermal (DTA) and roentgenphase (RPA) analyses. There have been used *Pt/Rh*-30/6- thermocouple at DTA, temperature determination accuracy is ±5*K*. RPA has been carried out on DRON-3 installation in $Cu_{k\alpha}$ radiation. There have been grown $TlIn_{1-x}Sb_xSe_2$ single crystals by Bridgemen-Stochbarger method at x=0.001; 0.003 and 0.0045. Grown compositions have high degree of monocrystalline and splitting along the direction (001) into thin needles.

Monocrystalline samples are used for study of photoresistive properties. $TlIn_{1-x}Sb_xSe_2$ crystals have p-type conductivity. Contacts are applied by *In* melting on splitting surface and provide ohmage volt-ampere characteristics (VAC) up to electric intensity ≤ 200V/cm. Indium contacts are differed by stability and provide high measurement accuracy of photoelectric parameters of $TlIn_{1-x}Sb_xSe_2$ crystals. Electric field is applied along the direction (001), and nonmodulated radiation flow is headed perpendicular to spall plane. Measurements are carried out at 300K, and voltage is taken within linear (ohmic) section of VAC. After measurement of spectral characteristics of photocurrents there have been carried out a compensation of light flows in quantum number with graduated germanium photodiode.

In Table 1 there have been presented values of resistance relation in darkness and light 200 lux for $TlIn_{1-x}Sb_xSe_2$ single crystals (R_d/R_l) at photon energy corresponding to photocurrent maximum ($h\nu_{max}$), also average values of integral photosensitivity (S_{ph}).

As it is seen from table 1 samples of mixed crystals have high sensitivity in intrinsic absorption band.

By increasing x from 0.001 up to 0.0045 the ration R_d/R_l increases from 1.8 up to 9.37. High values of integral photosensitivity (S_{ph}) of studied crystals show prospects of their use as phototransducers of different purpose.

Table 1

Average parameter values of photoresistors of $TlIn_{1-x}Sb_xSe_2$ -based crystals.

x	R_d/R_l	S_{ph} $\mu A \cdot lm^{-1}$	$h\nu_{max}$ eV
0	8.65	123.5	1.5
0.001	1.8	28.2	1.5
0.003	4.13	288.0	1.45
0.0045	9.37	110.5	1.4

It is of interest to reveal influence of partial substitution In→Sb on roentgendosimetric characteristics of crystals under study.

Roentgenconductivity and roentgendosimetric characteristics are taken for crystals of initial compound $TlInSe_2$ as well as for crystals of solid solution on its base corresponding to the substitution In→Sb.

Electric intensity in samples is 2.5÷25 V/cm. Source of roentgen radiation is the installation for roentgenstructural analysis of URS-55A-type with BSV-2 tube. Roentgen

radiation intensity is controlled by current variation in tube at each given value of accelerating potential in it during the measurement. Absolute values of roentgen radiation dose are measured by crystal dosimeter of DRGZ-2.

Roentgenconductivity coefficients characterizing roentgen-sensitivity of crystals under investigation are defined as relative change of conductivity under the effect of roentgen radiation on per-unit of dose, as:

$$K_\sigma = \frac{\Delta\sigma_{E,\theta}}{\sigma_\theta \cdot E} = \frac{\sigma_E - \sigma_\theta}{\sigma_\theta \cdot E}\left(\frac{min}{R}\right),$$

where σ_θ - is a conductivity in the absence of roentgen radiation: σ_E is a conductivity under the effect of radiation with E *(R/min)* dose intensity.

Values of certain above-mentioned characteristic coefficients of roentgenconductivity of crystals as initial compound $TlInSe_2$ as solid solutions on its base corresponding to substitution In→Sb are given in table 2 for different values of accelerating voltage (V_a) in tube and corresponding doses of roentgen radiation.

As it follows from the experimental data, the coefficients of roentgenconductivity K_σ in all investigated crystals decrease regularly with a dose increase as well with the rise of value of accelerating voltage V_a in roentgen tube. Drop of roentgenconductivity coefficient $K_\sigma(E, V_a)$ is especially in the range of comparatively low values of accelerating voltage and roentgen radiation dose. Above V_a=30÷35keV and E=10÷15 R/min the change of $K_\sigma(E, V_a)$ at subsequent rise of "V_a" and "E" is slight. One of the possible reasons of the observed regularities can be as follows: in investigated crystals especially at comparatively low accelerating voltages the roentgenconductivity appears to be due predominantly to radiation absorption in oversurface layer. And with the rise of radiation intensity there have been initiated to prevail a mechanism of surface-square recombination that leads to observed decrease of roentgenconductivity coefficient. As the accelerating potential increases the "effective hardness" of roentgen radiation rises by virtue of which the depth of its penetration into the crystal increases as a result of this the absorption-generation of free photo-(roentgeno) carriers in volume predominantly occurs and proportion of incident radiation on crystal passing through it increases. Namely by this reason probably as values of accelerating potential increase the observed decrease of roentgenconductivity coefficient and its dependence on radiation dose takes place.

We also studied roentgenampere characteristics of $TlInSe_2$, $TlIn_{0.9955}Sb_{0.0045}Se_2$, $TlIn_{0.999}Sb_{0.001}Se_2$ crystals at different "effective hardnesses" of radiation. From these data analysis it follows that a dependence of stationary roentgencurrent $\Delta J_{E,\theta}$ on roentgen radiation (E) has exponential character, i.e.

$$\Delta J_{E,\theta} = J_E - J_\theta \sim E^\alpha$$

Exponent of a given dependence is defined graphically from roentgenampere characteristics as tangent of an angle of dependence slope $lg\Delta J_{E,\theta}$ on lgE.

Along with above-mentioned general regularities from the data in the Table 2 the regular increase of exponent function value $\Delta J_{E,\theta} \sim E^\alpha$ "α" under other equal conditions as the partially substitution of three-valent indium cations for corresponding Sb cations is traced. As it substitutes there have been shown tendency to decrease of roentgeconductivity coefficient (K_σ), especially in the range of low intensities of soft (low V_a) roentgen radiation. Revealed empirical regularities can be very useful in the development of crystalline roentgendetectors on the base of crystals of a given system.

Table 2.

Roentgendosimetric characteristics of $TlIn_{1-x}Sb_xSe_2$ single crystals

Crystal composition	V_a keV	Dose intensity E, R/min	K_σ - min/R	α
$TlInSe_2$	25	0.75÷2.73	0.32÷0.2	0.68
	30	1.75÷10.22	0.143÷0.063	0.56
	35	3.75÷19.74	0.090÷0.044	0.54
	40	7.0÷38.8	0.064÷0.029	0.52
	45	10÷61.2	0.056÷0.021	0.50
	50	13.5÷78.0	0.048÷0.020	0.48
$TlIn_{0.999}Sb_{0.001}Se_2$	25	0.75÷2.73	0.278÷0.221	0.96
	30	1.75÷10.22	0.179÷0.082	0.58
	35	3.75÷19.74	0.1111÷0.517	0.55
	40	7.0÷38.8	0.0744÷0.0322	0.52
	45	10÷61.2	0.0604÷0.0238	0.48
	50	13.5÷78.0	0.0525÷0.0211	0.46
$TlIn_{0.9955}Sb_{0.0045}Se_2$	25	0.75÷2.73	0.129÷0.142	1.70
	30	1.75÷10.22	0.111÷0.05	0.71
	35	3.75÷19.74	0.073÷0.0425	0.67
	40	7.0÷38.8	0.051÷0.27	0.65
	45	10÷61.2	0.0484÷0.022	0.62
	50	13.5÷78.0	0.038÷0.020	0.60

[1] *E.M. Kerimova, S.N. Mustafaeva, A.B. Magerramov.* Nonorganic materials. 1997, v. 33, №11, pp. 1325-1326.
[2] *S.N. Mustafaeva.* Nonorganic materials. 1994, v. 30, №8, pp. 1033-1036.
[3] *A.Z.Abasova, E.M.Kerimova, G.A.Muradova, A.M. Pashaev.* Ionizing irradiation of photoresistors and diode structures on the base of $TlGaSe_2$ and $TlInSe_2$ single crystals. Institute Phys. Conf .Ser. №152 : Section H : single crystals and thin film devices. 1998, IOP publishing LTD. p.983-988.
[4] *S.N. Mustafaeva, M.M. Asadov, V.A. Ramazanzade.* Roentgen-ampere dosimetric characteristics of lithium-intercalated $TlGa(In)Se_2$ single crystals. Materials of the Conf. on Ternary and Multinary Compounds. Salford, United Kingdom. 8-12th Sept. 1997, pp.1.71.
[5] *S.N. Mustafaeva, M.M. Asadov, V.A. Ramazanzade.* Nonorganic materials. 1995, v. 32, 31, pp. 318-320.
[6] *O.Z. Alekperov, M.A. Aljanov, E.M. Kerimova.* Turkish Journal of Physics. 1998, v. 22, p.1.6.
[7] *E.M. Kerimova, S.N. Mustafaeva, R.N. Kerimov, G.A. Gadzhieva.* Nonorganic materials. 1999, v. 35, №10, pp. 1-2.
[8] *E.M.Kerimova, S.N.Mustafaeva, E.F.Bagirzade, D.A. Huseynova.* Roentgendetectors. Mater. Of PPMSS 99 Chernivtsi, Ukraine. Sept., 7-11, 1999, p. 279.
[9] *D.V. Gitsu, I.N. Grincheshen, N.S. Popovich.* Phys. Stat. Sol. (a) 1982, v.72, №1, p. K113-K116.
[10] *D.V. Gitsu, I.N. Grincheshen, N.S. Popovich.* Phys. Stat. Sol. (a) 1983, v.76, №1, p. K5-K7.
[11] *I.N. Grincheshen, N.S. Popovich, A.A. Shtanov.* Phys. Stat. Sol. (a) 1984, v.85, №1, p. K85-K88.
[12] *I.N. Grincheshen, N.S. Popovich.* Fizika tekhnika poluprovodnikov. 1985, v.19, №2, pp.230-233.
[13] *G.I. Stepanov, I.V. Voigros, B.S. Chinik and others.* Fizika tverdogo tela. 1975, v.17, №1, pp. 166-169.

E.M. Kərimova, S.N. Mustafayeva, S.İ. Mehdiyeva, Firuzə M. Haşımzadə

$TlInSe_2$-$TlSbSe_2$ SİSTEMİ MONOKRİSTALLARININ FOTO- VƏ RENTGEN HƏSSASLIĞI VƏ RENTGENAMPER XARAKTERİSTİKALARI

$TlIn_{1-x}Sb_xSe_2$ bərk məhlulunun tərkibinin onların foto- və rentgendozimetrik parametrlərinə təsiri öyrənilmişdir. Bütün öyrənilən tərkiblərdən $TlIn_{0.999}Sb_{0.001}Se_2$ monokristallarının rentgen keçirmə əmsalı (K_σ) qismən böyük qiymətə malikdir, məsələn: "effektiv sərt" şüalanmanın U_y=25keV və dozanin gücü E=0.278 R/dəq qiymətlərində K_σ=0.278dəq/R.

$TlIn_{1-x}Sb_xSe_2$ kristalının rentgenamper xarakteristikası göstərir ki, stasionar rentgen cərəyanın ($\Delta J_{E,\theta}$) rentgenşüalanmanın dozasından asılılığı üstlü xarakter daşıyır: $\Delta J_{E,\theta} \sim E^\alpha$. In→Sb qismən əvəzlənməsi və x-in artırılması nəticəsində α qiyməti artır. Belə ki, U_y=25÷50keV qiymətlərində $TlIn_{0.999}Sb_{0.001}Se_2$ üçün əgər α=0.96÷0.46, $TlIn_{0.9955}Sb_{0.0045}Se_2$ üçün isə α=1.70÷0.60 olur.

Alınan nəticələr göstərir ki, $TlInSe_2$-$TlSbSe_2$ sistemin rentgendefektorların hazırlanması üçün istifadə oluna bilər.

Э.М. Керимова, С.Н. Мустафаева, С.И. Мехтиева, Фируза М. Гашимзаде

ФОТО-И РЕНТГЕНОЧУВСТВИТЕЛЬНОСТЬ И РЕНТГЕНОАМПЕРНЫЕ ХАРАКТЕРИСТИКИ МОНОКРИСТАЛЛОВ СИСТЕМЫ $TlInSe_2$-$TlSbSe_2$

Изучено влияние состава твердых растворов $TlIn_{1-x}Sb_xSe_2$ на фоточувствительность и рентгенодозиметрические параметры. Из изученных составов наибольшее значение коэффициента рентгенопроводимости K_σ имели монокристаллы $TlIn_{0.999}Sb_{0.001}Se_2$, так например K_σ=0.278 мин/Р при "эффективной жесткости" излучения U_y=25 кэВ и мощности дозы E=0.278 Р/мин. Изучение рентгеноамперных характеристик кристаллов $TlIn_{1-x}Sb_xSe_2$ показало, что зависимость стационарного рентгено-тока ($\Delta J_{E,\theta}$) от дозы рентгеновского излучения (E) носит степенной характер: $\Delta J_{E,\theta} \sim E^\alpha$.

По мере частичного замещения In→Sb, т.е. с увеличением x, прослеживается увеличение величины показателя α. Так, если для $TlIn_{0.999}Sb_{0.001}Se_2$ α=0.96÷0.46, то для $TlIn_{0.9955}Sb_{0.0045}Se_2$ α=1.70÷0.60 при U_y=25÷50кэВ. Полученные результаты показали, что кристаллы системы $TlInSe_2$-$TlSbSe_2$ могут быть использованы для создания рентгенодетекторов.

Received: 28.12.01

THE INFLUENCE OF THE THERMOPROCESSING ON DEFORMATION PROPERTIES AND PHYSICAL STRUCTURES OF POLYMER COMPOSITIONS

T.M. VELIEV, S.A. ABBASOV, M.J. ZEINALOVA, Z.C. EFENDIEVA
Institute of Physics of the Azerbaijan National Academy of Sciences
H. Javid av. 33. Baku. 370143

The influence of the preliminary thermoprocessing on deformation properties and the physical structure of polypropylene and polyethylene of the low density (PELD) compositions with different submolecular structures has been studied. It has been shown, that the value of the relative deformation ε % on the stretching reduces depending on the duration and the temperature of the preliminary thermoprocessing. It is explained by the change of the physical structure, i.e. by the growth of the crystallization degree in slow-cooling (SC) and quick-cooling (QC) samples of PP-PELD compositions.

The experimental results of physical-mechanical characteristics research of polymer composite materials may be divided into 3 groups unequal by the amount of data. The first is the large collection of results, obtained for polymer composition at different concentrations of various fillers [1]. This conclusion has found the practical reflection in formulations of worked-out materials, in which the dispersed fillers content does not exceed 30 mass % [2]. Compositions with the high fillers concentration have comparatively recently appeared and their properties are considerably distinguished from initial polymers characteristics. As a rule, they are materials with the high module, but with low breaking characteristics. The second data group is separate examples, demonstrating the opportunity of the high deformational characteristics achievement at the high fillers content. So, high-molecular polyethylene (HMPE) compositions, which are deformed up to 30 % at the fillers content 50-60 mass %, are obtained by the method of polymerized filling [3,4]. Compositions, worked out by Sapcofile firm, represent the polypropylene, filled up to 50 mass %. From series of materials one has the relative stretching at the breakdown up to 50 %, while this value does not exceed 30 % at rests.

Data analysis of physical-mechanical properties shows, that the third group of composition materials, i.e. compositions on the base of polymer-polymer, have the essential distinctions in values of the hardness, creep, elasticity module, deformational heat-resistance indices. It is worth to mention, that these classes of compositional materials are also essentially distinguished by the production volume and the price [5].

Growing demands to polymer materials dictate the necessity of the working-out of compositions with the complex of optimal properties. Special demands to the form and structure retention at high temperatures are presented to them at the use of the polymer compositional material in electron apparatus products. Therefore the research of thermal effect influence on deformational properties and the physical structure of PP-PELD 80:20 mass % compositions is the important problem, since it has been earlier shown by us, that PP-PELD compositions possess by optimal stable and deformational properties [6,7] exactly at such components relation.

The thermoprocessing has been carried out at temperatures 343, 353, 363 and 383 K during 0.5, 1, 1.5 and 2 months. The heat effect on polymer compositions films has been realized by thermostatic processing in the air atmosphere in the thermocabinet, after that the relative deformation ε % on the stretching has been measured, the value of the crystallization degree C of initial components and compositions, exposed to the thermal effect versus the thermoprocessing temperature and duration, has been determined. Samples crystallization degree C has been determined by method [8] with the exactness up to 6 %, as the square relation under the crystal peak (S) to the hole square ($S+S$) under the curve with the exclusion of the background and value of these results are given in tables 1 and 2:

$$K_S\% = \frac{S_K}{S_K + S_A}.$$

Table 1.

Values of the crystallization degree of initial components and PP:PELD=80:20 mass % compositions are preliminary exposed to the thermal effect at different processing temperatures T:

Regime of samples receipt	PP Initial	PELD initial	PP:PELD = 80:20 Initial	PP:PELD = 80:20, t =2 months at different T , K			
				343	353	363	383
Slow cooling	70	60	65	70	74	82	87
Quick cooling	48	40	38	41	44	49	55

It is seen from tables 1 and 2, that the crystallization degree of SC and QC compositions increases with the growth of T (at the constant t) and t (at the constant T).

Curves of relative deformation dependences ε % on the stretching on the temperature T of the deformation measurement for initial and preliminary exposed to the thermal effect of slow-cooling (SC) samples of PP:PELD=80:20 mass % composition at different processing temperatures T during 2 months and during different thermo-processing T durations at the temperature 383 K, respectively, at the other equal conditions (σ =10 Mpa, t = 6 sec., at the constant temperature) are presented on fig. 1 and 2.

Table 2.

Values of the crystallization degree of initial components and PP:PELD=80:20 mass % compositions are preliminary exposed to the thermoprocessing at different thermal treatment durations t

Regime of samples receipt	PP initial	PELD initial	PP:PELD=80:20 initial	PP:PELD=80:20, at T = 383 K, in different t, a month			
				0.5	1	1.5	2
Slow cooling	70	60	65	68	71	79	87
Quick cooling	48	40	38	39	42	46	55

It has been established on the obtained thermomechanical curves base, that, first, the value of ε % on the stretching of SC composition samples, in both cases, beginning with the temperature 353 and 363 K increases with the growth of the measurement temperature. Second, at measurement temperatures constants ε %, at which the large deformations are observed, the value ε % on the stretching reduces with the growth of the preliminary processing temperature T and the thermoprocessing duration t.

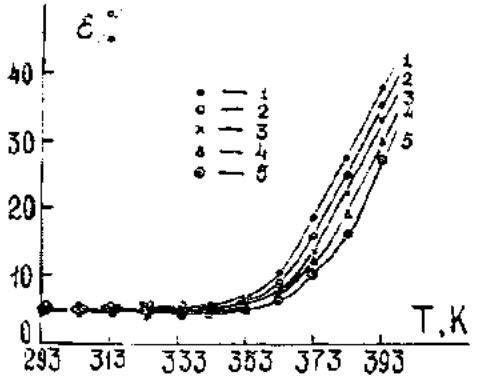

Fig.1. Thermomechanical curves of slow-cooling PP:PELD= =80:20 mass % composition, treated at various temperatures during 2 months:1 - initial, 2- T =343 K, 3 - T =353K, 4 - T =363 K, 5 - T =383 K

Dependences of ε % on the stretching on the preliminary processing temperature T for SC samples of the optimal composition, exposed to thermal effects during 2 months are presented on fig.3. This dependence is constructed on the base of thermomechanical diagrams, given on fig.1. It follows from fig.3, that noticeable reductions of ε % on the stretching of SC samples of the optimal composition versus T at other equal conditions, are observed higher the glass temperature. It is seen analogously from fig.2, that the value of ε % on the stretching versus the thermoprocessing t duration also reduces.

So, it has been shown at the given research stage, that changes of ε % on the stretching both depending on the preliminary thermoprocessing temperature, and thermoprocessing duration are uniform. Corresponding data for quick cooling (QC) samples of the optimal PP:PELD=80:20 mass % composition are similar.

Obtained results (for SC composition samples, fig. 3) allow to assume, that the maximal reduction of ε % on the stretching of SC and QC samples of the optimal composition versus T at the temperature of the deformation measurement 383K makes ~27% and 40%, respectively. Observed reduction of ε % on the stretching of SC and QC samples of PP:PELD=80:20 mass % composition versus T are the result of the fact, that the crystallization degree grows at the thermal effects in them.

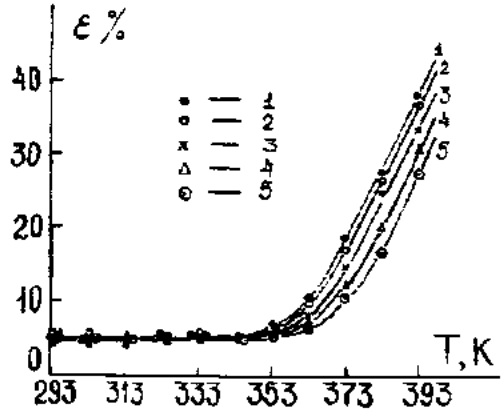

Fig.2. Thermomechanical curves of slow-cooling PP:PELD= =80:20 mass % composition , treated at T= 383 K at various thermoprocessing durations: 1- initial, 2 - t =0.5 months,3 - t=1 month, 4 - t=1.5 months, 5- t =2 months

The research of the deformational properties dependence on thermoprocessing conditions has also shown, that the reduction of ε % on the stretching of SC and QC samples of the optimal composition is observed with the growth of the temperature and the thermoprocessing duration. So, at the treatment temperature 383 K and the thermoprocessing duration during 2 months ε % on the stretching for SC sample falls from 27% to 7%, and for QC sample- from 40% to 17%.

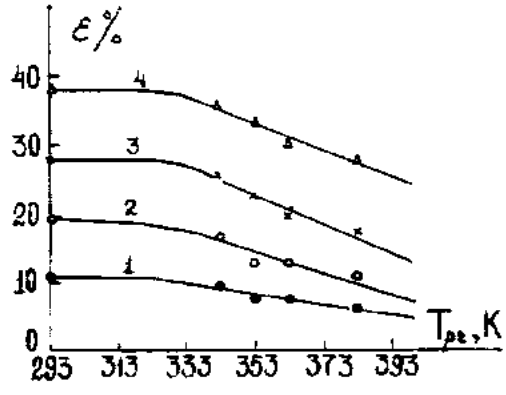

Fig. 3 Relative deformation ε % dependence of slow-cooling PP:PELD=80:20 mass % compositions samples, treated during 2 months, on the thermal treatment temperature: 1- T =363 K, 2- T =373 K, 3- T =383 K, 4- T =393 K.

Therefore, obtained experimental results show, that reductions of deformational and thermotechnical properties

occur at the thermal effect on the polymer PP:PELD=80:20 mass % composition and the nature of these changes depends on the temperature and the thermoprocessing duration. It has been shown at the result of structural researches, that the physical structure of the initial SC PP:PELD=80:20 mass % composition is characterized by rather high crystallization degree (α=65%), and QC PP:PELD=80:20 mass % composition- by relatively low crystallization degree (α=88 %, table.1 and 2). As it is seen from tables 1 and 2, the crystallization degree grows versus the temperature and samples thermoprocessing duration. For example, the crystallization in SC and QC samples of PP:PELD=80:20 mass % increases up to 87 % and 55 % after the thermal effect at 383 K during 2 months, respectively, and it is gone with the considerable growth of the samples density, with the increase of the crystallization size. Above-molecular regularity grows. And, on that reason the relative deformation value of ε % on the stretching reduces at the samples thermoprocessing of PP:PELD=80:20 mass % compositions.

Therefore, it follows from aforesaid, that the stability of polymer compositional materials to the thermoprocessing and the nature of deformational properties changes are explained by the growth of the crystallization degree.

[1] "Fillers for polymer compositional materials"-Under edition of *G. S. Catz. D. V. Milevski*, M:"Chemistry", 1981.

[2] Application of polyolefins, polystyrenes, fluorine plastic, polyvinylacetate plastics"-Catalogue. Cherkass, 1987.

[3] *E. G. Hovard, R.D. Lipscomb*. Ing. Tng. Chem.: Prod. Res. Dev., 1994, v.20, №1,pp. 421-427.

[4] *F. S. Dyachkovskii, A. A. Novokshonova* " Chemistry successes", 1989, v.53, №2, pp. 200-220.

[5] Engineering Plastics. "European plastics News", 1984, v.11, №6, pp. 7-14.

[6] *T. M. Veliev, M. J. Zeinalova, S. A. Abbasov, I. K. Alieva, S. S. Bedirkhanova*. Fizika, 2000, art. 5, №4, pp. 55-58.

[7] *T. M. Veliev, M. J. Zeinalova, S. A. Abbasov, I. K. Alieva, S. S. Bedirkhanova*. Fizika, 2000, art. 6, № 2, pp. 10-13

[8] *M. A. Uartikov, K. A. Vilegjanina*. " Polymers roentgenography" L: "Chemistry", 1972, p.96.

T.M. Vəliyev, S.A. Abbasov, M.C. Zeynalova, Z.Ç. Əfəndiyeva

TERMİK İŞLƏNMƏNİN POLİMER KOMPOZİSİYALARININ DEFORMASİYA XASSƏLƏRİNƏ VƏ FİZİKİ QURULUŞUNA TƏSİRİ

Termik işlənmənin müxtəlif üst molekulyar quruluşa malik polipropilen aşağı sıxlıqlı polietilen kompozisiyalarının deformasiya xassələrinə və fiziki quruluşuna təsiri öyrənilmişdir. Göstərilmişdir ki, ε % nisbi dartılma deformasiyasının qiyməti termik işlənmənin müddətindən və temperaturundan asılı olaraq azalır. Bu, fiziki quruluşun dəyişməsi ilə, yəni yavaş soyudulmuş və tez soyudulmuş kompozisiya nümunələrində kristallaşma dərəcəsinin artması ilə izah olunur.

Т.М. Велиев, С.А. Абасов, М.Дж. Зейналова, З.Ч. Эфендиева

ВЛИЯНИЕ ТЕРМООБРАБОТКИ НА ДЕФОРМАЦИОННЫЕ СВОЙСТВА И ФИЗИЧЕСКУЮ СТРУКТУРУ ПОЛИМЕРНЫХ КОМПОЗИЦИЙ

Изучено влияние предварительной термообработки на деформационные свойства и физическую структуру композиций полипропилен – полиэтилен низкой плотности (ПП-ПЭНП) с различными надмолекулярными структурами (НМС). Показано, что значение относительной деформации ε % на растяжение уменьшается в зависимости от длительности и температуры предварительной термообработки. Это объясняется изменением физической структуры, т.е. увеличением степени кристаллизации в медленно охлажденных (МО) и быстро охлажденных (БО) образцах композиции ПП-ПЭНП.

Received: 22.10.01

THE DETERMINATION OF THE NATURE OF DEEP LEVELS IN SILICON *p-n* JUNCTIONS

S.G. RZAYEV, Z.M. ZAKHRABEKOVA
Institute of Physics of the Azerbaijan National Academy of Sciences
H. Javid av. 33, Baku, 370143

Dependences of the deep levels (d.l.) recharging time constant on the temperature (T) are determined by methods of the deep levels transient spectroscopy (DLTS). The nature of d.l. in *p-n* junction of silicon integrated circuits is revealed without destroying their structures.

Deep levels in the forbidden band of semiconductors have the considerable influence on parameters of semiconductor devices, in particular, they determine such important parameters of *p-n* junctions, as the leakage current, breakdown voltage, the carriers lifetime, etc. It is necessary to reveal the nature and carry out more detailed research of their properties and determination of parameters for working out the model notion about their influence mechanism on electron processes in semiconductors.

Methods of thermostimulated currents (TSC) shown to be rather effective at the same time are simple research methods. Parameters of d.l. in silicon planar *p-n* junction have been revealed and determined in [1] with the help of these methods. Though they allow to reveal and estimate d.l. parameters these methods are insufficient for determination of their nature. Therefore it is necessary to search for methods allowing to determine the nature and to define d.l. parameters in p-n junctions more precisely. Methods of DLTS have such properties. They are distinguished by the high sensitivity and resolvability capacity and also by the simplicity of the results interpretation, what is particularly important for the determination of the d.l. nature.

In the present work d.l. in *p-n* junctions of integrated circuits (IC) of the high integration are revealed and studied by methods of DLTS and on the base of this study before unknown nature of d.l. is revealed and their parameters are determined more precisely.

Methods of the experiment and a discussion of results

Research has been carried out on planar silicon p-n junctions, whose section is represented in [2]. The basic region of the junction consists of the part of the epitaxial film of the (111)-surface of the ≈2.1mkm thickness alloyed by boron (≈$5\cdot10^{16}$cm^{-3}). The collector region consists of the n - layer, formed in the *p*-substrate of the As (10^{20}cm^{-3}) diffusion, and the vertical n – layer attached to it created in the epitaxial film by the phosphorous (≈$5\cdot10^{18}$cm^{-3}) diffusion, which exits to the film surface.

Deep levels were revealed in studied *p-n* junctions of high leakage currents by TSC methods and their parameters were determined: the activation energy is E_t=(0.24±0.003)eV, a section of capture is σ=(3÷5)$\cdot10^{-20}$cm^2, the d.l. concentration is Nt= (1÷5)$\cdot10^{16}$cm^{-3} [1].

Although the TSC method is very informatic and technically simple, it has a number of shortcomings, one of them is the impossibility of the simultaneous determination of σ and N_t. Another essential shortcoming of this method is the fact, that parameters of d.l. are calculated by the form and peaks position of TSC on the temperature scale, on which the rate of the sample heating, the degree of the initial centers filling and the value, attached to the sample the electric field, have the noticeable influence. Therefore, as a rule, the other independent method is applied at the use of TSC method for the check of obtained results and the receipt of the additional information. The method of DLTS is applied as the control method in the present work, which allows to determine σ and N_t simultaneously and also to find the dependence of the d.l. recharging time on the temperature, what is particularly important for the determination of the d.l. nature, as it will be shown below.

The main point of the DLTS method consists of the following:

This method is the particular case of the capacitance spectroscopy, based on the measurement of capacity changes of *p-n* structures, caused by the recharging of d.l. in the space charge layer. If the inverse bias is given to *p-n* junction, then all free carriers (in given case electrons) for the time of 10^{-10}s order will escape the space charge layer (SCL) to the region of the electrical neutrality and capture processes on d.l. will be practically excluded in the region of the SCL; i.e. processes of the carriers emission from the level will dominate, that leads to the change of the charged centers concentration in the SCL.

If the inverse bias is removed, the electrons will return to the depletion region and the process of their capture on the d.l. will start. If holes are introduced in the studied region with the previously filled centers, then the process of their capture will be dominating. And, at last, if centers are devastated and all free carriers are removed from the depletion region, then the process of the holes emission from d.l. will dominate. As it is seen from above-mentioned, variating the bias voltage, given to *p-n* junction, the conditions may be created, under which the charge of the ionized centers concentration in the SCL will be determined by a single process. The change of the ionized centers concentration in the SCL is externally manifested through the capacity change. The d.l. recharging occurs with some time constant, which exponentially depends on the energy activation E_t of the level and on the temperature T [3]:

$$\tau_{r.c} = \left(\sigma_n \vartheta_T N_c\right)^{-1} exp\left(\frac{E_c - E_t}{KT}\right) \qquad (1)$$

where σ_n is the cross section of the electron capture on the d.l., ϑ_T is the heat velocity of the electron, N_c is the state density in the conduction band.

The relation between the capacity charge, the d.l. concentration and the constant of the recharging time is determined from the Poisson equation:

$$div\overline{E} = \frac{\rho}{\varepsilon_0 \varepsilon_s} \qquad (2)$$

where $\overline{E}$ is the electric field strength, ρ is the charge density, ε_s is the dielectric constant of the semiconductor. The particular solution of this equation is given in [3,4]. Both the constant of the recharging time of the d.l. and the section of the carriers capture may be determined by the choice of the experiment conditions, and the energy activation of the d.l. may be determined by the slope of $ln(\tau T^2) \sim 1/T$ dependence from [1]

It follows from [1], that the recharging time constant of the d.l. depends on both the activation energy and the carriers capture cross-section. The $\tau(T)$ dependences are different for two d.l. with the identical activation energy in the consequence of this. This dependence is applied as the main distinctive sigh of the impurity. The unknown d.l. is identified by the coincidence of the (T) dependence for all levels with corresponding dependences for one of known impurities.

Two methods of DLTS are distinguished depending on the measured quantity:

1. The constant voltage when the capacity transient is measured at the constant bias voltage in p-n junction.

2. The constant capacity when the capacity of the *p-n* junction is supported by the constant and the change of the bias voltage, backing the capacity constant, is measured.

The capacity, the width of the SCL and the concentration of ionized d.l. are changed depending on the time in the case of the constant voltage (the capacity transient), what makes the measurement of d.l. parameters difficult in the case of the heterogeneous distribution of shallow and deep levels in the semiconductor volume. The method of the capacity constant (the voltage transient) where not changes of the barrier capacity in the time are registered, but the voltage change, lacks this shortcoming.

The compensated method, in which the tracking system automatically compensates the capacity change in the time, is caused by the d.l. ionization by the means of the supply of small compensated increments of the voltage on the sample, is the most convenient from different registration methods of voltage changes. The mentioned method allows to unite the transient filtration with the defined time constant and to support the capacity constant in the time. This method allows to measure the quick voltage transient ($\tau = 10^{-6} \div 10^{-1}$s).

The principal scheme of the device, on which the compensated registration method of voltage changes is realized on the barrier, is shown on fig.1. The description and its advantages over other capacity research methods of d.l. are shown in [4,5].

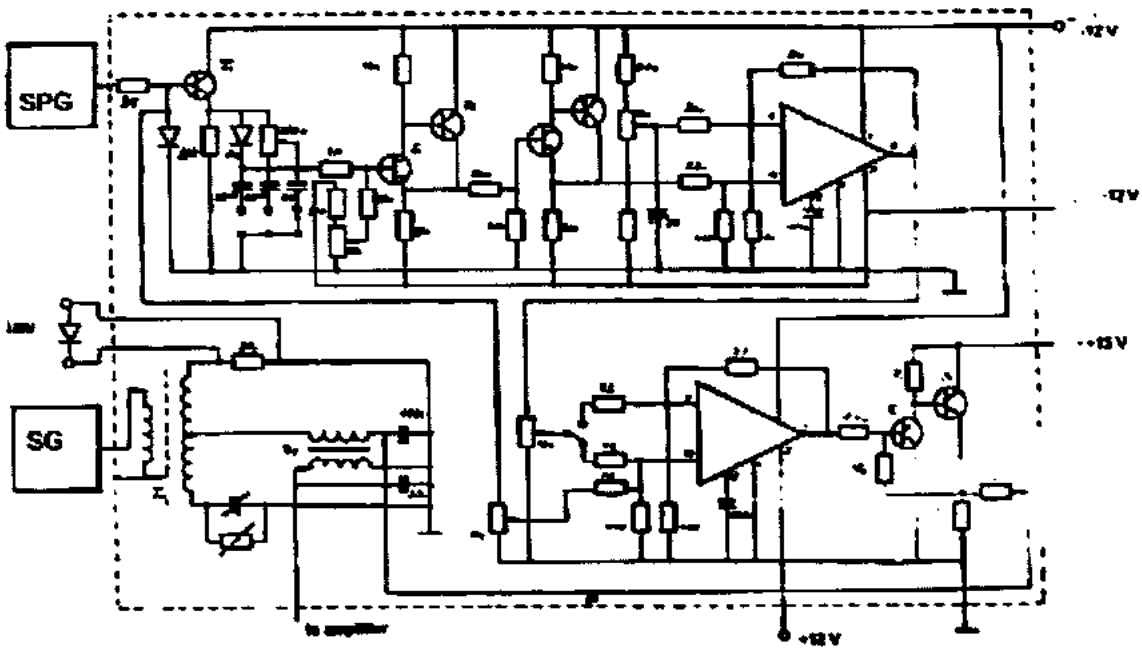

Fig.1 The principal scheme of the compensated device for the transient registration of the voltage on the *p-n* junction.

The regulating voltage during changes with the time changes according to the exponential law at the d.l. recharge:

$$u(t) = u_0 exp(-t/\tau_{r.c.}) \qquad (3)$$

where $u_0 = q/\varepsilon \int_0^{x-\lambda} N_t x dx$. x is the thickness of the depletion region, $\lambda = \sqrt{2\varepsilon(E_F - E_t)/q^2 N_s}$; N_s is the concentration of shallow impurities, q is the electron charge, exponential impulses (EI) of the voltage $u=u_{EI}\ exp(-t/\tau_{EI})$ with the fixed time constant τ_{EI} are synchronously delivered on samples along with the rectangular impulses of the inverse bias and it is necessary to fulfill the conditions $u_0=u_{EI}$, in order that the diode capacity remains constant in the recharging process at $\tau_{r.c.}=\tau_{EI}$.

The fulfillment of these conditions is provided by the fact, that the EI amplitude is persistently regulated by the slow feed-back, keeping the bias at minimum.

As it has been noted above, the constant of the recharging time changes with the temperature change according to the law (1). The value $\tau_{r.c.}$ is determined by the condition, that each extremum on $\tau_{El}(T)$ dependences corresponds to the d.l., possessing by the recharge time $\tau_{r.c.}$ at the given temperature.

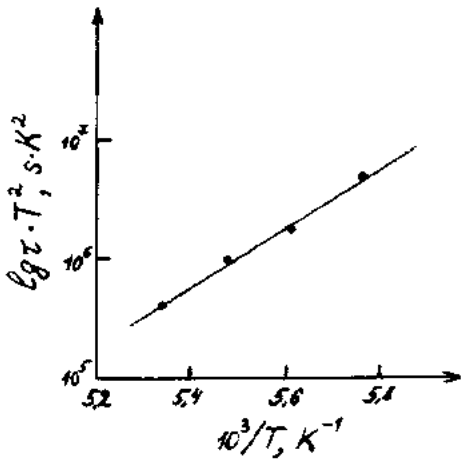

Fig. 2 Dependence of $lg(\tau T^2) \sim 1/T$ for p-n junctions with deep levels.

Therefore, the d.l. spectrum in the forbidden band may be determined from [1] at the smooth change of the temperature.

The Arrenius dependence $lg(\tau T^2) \sim 1/T$ for the *p-n* junction with high leakage current is shown on fig.2. D.l. have been earlier revealed by us by TSC methods in these samples and it has been established, that they increase the leakage current in $10^2 \div 10^3$ times, and also reduce the breakdown voltage in 0.4[illegible] in [1,6,7]. However, the nature of d.l. has remained obscure.

The main parameters of revealed d.l. have been determined by the analysis of the obtained Arrenius dependence (fig.2), using formula (1).

The activation energy is E_t=0.24eV, the capture cross-section is σ=3.5 $\cdot 10^{-20}$cm^2, the emission coefficient is $e_n = 1.2 \cdot 10^2 e^{-1}$ K^{-2}, the d.l. concentration is $(1 \div 5) \cdot 0^{16}$cm^{-3}, the capture coefficient is $\gamma = 5 \cdot 10^{-14}cm^{-3} \cdot$s^{-1}. Obtained values completely agree with values of appropriated parameters, obtained by TSC methods. It witnesses the reliability of the obtained results.

The analysis of the (T) dependence and also parameters for d.l. of the activation energy E_t=0.24eV has shown, that they coincide with analogous parameters for impurity atoms of the copper in the silicon [8,9]; i.e. revealed d.l. are caused by atoms of the copper. The quartz, applied in industrial devices, may serve as the possible pollution source of the serial IC.

Conclusion

Thus, applying the suggested method of $\tau(T)$ determination in the given work, the d.l. parameters may be exactly determined by DLTS methods and the identification may be carried out with parameters of known impurities without destroying *p-n* structures.

Obtained data may be applied for more accurate definition of model notions about the d.l. influence on electron processes in semiconductors, and also for the correction of the technological production process of semiconductor devices.

[1] *S.G Rzayev, A.G. Abdullaev.* Izv AN. Az.SSR: series of physico-technical and math. sciences; 1983, №2, pp.70-73.

[2] *S.G. Rzayev, E. P. Nakhmedov.* FTT, 1993, v.35, №4, pp. 1038-1042

[3] *J.A. Pals.* Sol. St., a, 1974, v. 17; №11, p.1139

[4] *S.G. Rzayev.* Principles of the capacitance spectroscopy of deep centers. IFAN, Az. SSR. Preprint №24: Baku.1987.

[5] *V.Y. Prince, K.G. Bulatetskii.* PTE, 1979, №4, pp. 205-258.

[6] *S.G. Rzayev.* E.T: series semiconductor devices, 1996, issue 6, pp.34-37

[7] *S.G. Rzayev.* Inorganic materials, 1998, №12, pp. 1415-1419.

[8] *L.S. Berman.* A.A. Lebedev. The capacitance spectroscopy of deep centers in semiconductors. "Nauka", L., 1981.

[9] *A.G. Milns.* "Impurities of deep levels in semiconductors". Mir. M., 1977.

S.Q. Rzayev, Z.M. Zöhrəbəyova

SİLİSİUM *p-n* KEÇİDLƏRİNDƏ DƏRİN SƏVİYYƏLƏRİN TƏBİƏTİNİN TƏYİN EDİLMƏSİ

Dərin səviyyələrin (d.s) yük dəyişməsinin zaman sabitinin temperaturdan asılılığının d.s. relaksion spektroskopiya (DSRS) metodu ilə təyin etmənin üsulu verilib. Bu üsul ilə silisium inteqral sxemlərin *p-n* keçidlərində d.s. təbiəti təyin edilib və onların mis atomlarına aid olduğu təsbid edilib.

С. Г. Рзаев, З. М. Захрабекова

ВЫЯСНЕНИЕ ПРИРОДЫ ГЛУБОКИХ УРОВНЕЙ В КРЕМНИЕВЫХ *p-n* ПЕРЕХОДАХ

Методами релаксационной спектроскопии глубоких уровней (РСГУ) определены зависимости постоянной времени перезарядки глубоких уровней от температуры $\tau(T)$. Выяснена природа глубоких уровней в p-n переходах кремниевых интегральных схем, не разрушая их структуры.

Received: 11.10.01

PECULIARITIES OF PHOTOELASTIC EFFECT AND SOME IDEAS ON THEIR APPLICATION

A.R. HASANOV

Institute of Physics of the Azerbaijan National Academy of Sciences
H. Javid av. 33, Baku, 370143

The peculiarities of acoustic -optic interaction in photoelastic media are analyzed in a context of their application for a solution of some radio electronic problems

1. GENERAL INFORMATION

At an excitation of an acoustic wave in a photoelastic medium there are dynamic modifications of an index refraction (density of a medium) occur. These modifications lead to the formation of a moving diffraction grating, whose step is equal to the acoustic wavelength, and the amplitude is proportional both to the amplitude of an acoustic wave, and to the photoelastic constant of the medium. At passage through such media, a number of parameters of an optical wave varies (modulates). This phenomenon is called as the effect of acoustic-optic interaction or photo-elastic effect. Acoustic-optic modulator is the device for realization of this effect. At the same time the title "acoustic light modulator" in the literature is often used. Acoustic-optic modulator consists of a photoelastic medium, to one edge of which an electro - acoustic transducer (EAT) is attached. EAT transforms an input electrical signal into an acoustic wave spreading in the photoelastic medium with a velocity, approximately, in 10^5 times less than the velocity of propagation of an electromagnetic wave.

Peculiarities of acoustic-optic interaction can be used for a solution of many problems of radio electronics.

The purpose of the present work is the analysis and evaluation of potential possibilities of photoelastic effect in a context of application of its peculiarities for signals processing.

2. PECULIARITIES OF PHOTOELASTIC EFFECT

Owing to acoustic-optic interaction an incident optical wave diffracts on dynamic modifications of the density of photoelastic media. Thus, the intensity, propagation direction and frequency of optical wave in diffraction order are defined by parameters of an electrical signal brought to terminals of the electro -acoustic transducer. Moreover, the response of the photodetector, disposed on a path of the diffraction order, lags from action on an electrical input on the time

$$\tau = x/\vartheta \quad , \qquad (1)$$

where x is a distance from the electro -acoustic transducer up to a point of the acoustic-optic interaction; ϑ is a velocity of propagation of elastic waves in the photoelastic medium.

Depending on a geometry and character of acoustic-optic interaction, diffractions of Raman-Nath and Bragg are distinguished. The basic external difference of Bragg diffraction from Raman-Nath diffraction consists of a unsymmetrical emerging of diffraction orders, with modification of the incidence angle θ_0 of a light beam in the aperture of the acoustic-optic modulator. Thus, the maximum of the light intensity in the diffraction order takes place if the light falls on the aperture of the acoustic-optic modulator at the Bragg angle, i.e. when $\theta_0=\pm\theta_B$. The Bragg angle is defined from the relation

$$\sin\theta_B = \lambda/(2\Lambda), \qquad (2)$$

where λ is the wave length of the incident light; Λ is the elastic wavelength in the photoelastic medium of the acoustic-optic modulator.

Acoustic-optic devices, using the Raman-Nath diffraction, have been extensively applied in systems of signal processing on frequencies up to 100 MHz. The Bragg diffraction is widely applied in acoustic-optic systems of signal processing working in the frequency region from a few tens of MHz up to units of GHz.

Application of acoustic-optic modulators, where the Bragg diffraction is used, allows to raise some technical characteristics of acoustic-optic devices, for example: the central frequency of a pass band; light intensity in a diffractional order etc.

It is established, that the intensity I_l of a deviating light in the Bragg diffraction mode is directly proportional to the square of input voltage U_a [1]:

$$I_l = BU_a^2 \qquad (2)$$

where B is the constant factor. Accordingly, the output voltage of the photodetector with the definite precision repeats the law of a modification of amplitude of the input voltage.

At $\theta_0=\pm\theta_B$, with increase of the frequency of an acoustic wave, diffractional effects of higher orders disappear and only light beams of zero and first orders are predominating. The diffractional order spread under the angle θ_d, defined from the relation

$$\sin\theta_d + \sin\theta_0 = \lambda/\Lambda \qquad (4)$$

Assuming, that the incidence angle θ_0 of the light beam on a surface of the photo-elastic medium is constant, i.e. $\theta_0=\pm\theta_B=const$, where θ_{B0} is the Bragg angle on the central frequency F_0 of the input action, from the joint analysis (2) and (4) it is possible to receive the following expression for the diffraction angle θ_d at the Bragg condition:

$$\sin\theta_d + \sin\theta_0 = \lambda/\Lambda \, , \qquad (5)$$

where F is the frequency of the elastic wave in the photoelastic medium.

The equation (5) indicates that the angle of deflection θ_d is variable versus the frequency F of elastic waves in a photo-elastic medium, and therefore also versus the frequency of the input electrical signal. From (5) for small modifications of the diffraction angle $\Delta\theta_d$ (where $sin\Delta\theta_0 \approx \Delta\theta_B$.), it is possible to receive the following expression:

$$\Delta\theta_d = 0.5\lambda \cdot \Delta F / \vartheta \ . \qquad (6)$$

where $\Delta F = F - F_0$.

According to (6), in the Bragg condition a modification of an angle of diffraction is in the rectilinear dependence on a frequency modification of an input action.

After acoustic-optic interaction the frequency ω_d of the light beam in a diffractional order is shifted due to Dopler effect on the magnitude $\Omega = 2\pi F$ and is defined as:

$$\omega_d = \omega \pm \Omega \ . \qquad (7)$$

where ω is the angular frequency of light in the photo-elastic medium.

3. APPLICATION OF PECULIARITIES OF PHOTOELASTIC EFFECT

The analysis of relations (1) and (3) allows to postulate, that a signal given on the electrical input of the acoustic-optic modulator and extracted through the photo-elastic connection on a distance x from the electro-acoustic transducer receives the temporal delay τ defined by the relation (1). In other words, at feed of the following amplitude - modulated signal to terminals of the electro-acoustic transducer

$$U_1(t) = U_0[1 + M \cdot s(t)] cos\Omega t \qquad (8)$$

where U_0 is the amplitude of the no modulated carrier; M is the index of the amplitude modulation; $s(t)$ is the modulating process on the output of the photodetector, we obtain:

$$U_2(t) = c \cdot s(t - x/\vartheta) \qquad (8)$$

where C is the constant factor. Thus, the indicated delay linearly depends on x and can be changed in large limits. For example, if we use TeO_2 as the photo-elastic medium, where the velocity of the slow shift wave is equal to 617m/s, then at x=2cm we receive τ=32mcs (TeO_2 allows to receive the temporal aperture ≈80mcs). Therefore, the smooth modification of x from 0 up to 2 cm will be accompanied by a smooth control of the delay time of the output signal from 0 up to 32 mcs accordingly. The modification of the indicated distance can be carried out by mechanical, electromechanical and electronic [2,3] methods.

The adduced numerical example shows, that the low acoustic velocity is favorable at construction of acoustic-optic delay lines. Let's mark, that in crystals of halogens of mercury (in particular, Hg_2Br_2 and Hg_2Cl_2) the velocity of a sound is 2 times less, than in TeO_2 [4].

According to relation (6), the modification of the frequency of input action is accompanied by a linear modification of a diffraction angle in space, as a result each direction of a light diffraction (in the plane xz) corresponds to definite frequency of input action (fig.1). This peculiarity of the Bragg diffraction can be used for detection of frequency - modulated signals [5], the spectral analysis of broadband signals. The work of the panoramic receiver [6], receiver of line frequency -modulated signals [7] is founded on this principle. This peculiarity can be used, also, for reading of an information from the storage device in acoustic-optic transformators of a temporal scale of signals [8]. Low acoustic velocity is favorable in these devices also on cause, that allows to receive large angles of a deviation and secures high resolution on the frequency. At the same time it does not allow to receive large velocity of a deviation.

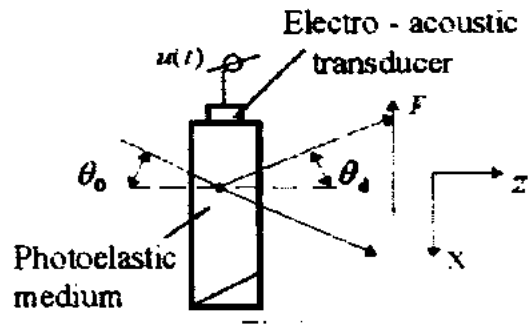

Fig.1

Caused by Dopler effect, the shift of frequency of a light wave in a diffractional order can be used for restoring of the radio-frequency signal operating on the input of the acoustic-optic modulator, by optical heterodyne of the diffracted light beam by a part of the incident or undiffracted light (appearing in a role of the local heterodyne) [9,10]. In this case, if an amplitude-modulated signal (8) is brought to terminals of electro -acoustic transducer, we have on the output of the photodetector:

$$u_2'(t) = c' U_0 \left[1 + M \cdot s(t - x/\vartheta)\right] \cdot cos\,\Omega(t - x/\vartheta) \ . \qquad (10)$$

where C' is constant factor.

We mark, that the heterodyne method of registration of an optical signal allows to increase sensitivity of a photoreception device on 3-4 orders in comparison with the direct detection and approaches this sensitivity to the quantum limit.

CONCLUSION

The above mentioned examples on application of peculiarities of acoustic-optic effect show, that development of effective electro -acoustic transducers and photo -elastic media with high refraction factor will allow to synthesize simple devices solving highly difficult problems. We mark, that acoustic-optic modulator have been already developed, requiring only some tens mW on the electrical input for security of effective acoustic-optic interaction. The important virtue of acoustic-optic methods of signals processing is that the device used for a solution of one task can be easily adapted for solution of other. For example, devices of a delay of signals can be used also, as the acoustic-optical frequency detector, by placing of the diaphragm with the cuneiform orifice on a path of the diffractional order.

A.R. Gasanov. Basis of theory and technique of formation and processing of signals by acoustic-optic methods. Baki:. ELM, 1999, 55p. (in Russian).

[1] *A.R. Gasanov*. "Radioelectronica", 2000, №5, p.73-75. (in Russian).

[2] *A.M. Pashaev, A.R. Gasanov, A.A. Mamedov and Kh.I. Gasanov*. "Pribori i sistemi upravleniya", 1997, №6, p.46. (in Russian).

[3] *A.P. Goutzoulis and M.S. Gottlieb*."Design and performance of optical activity based Hg_2Cl_2 Bragg gells."Proc. SPIE, vol.936, Advances in Optical Information Processing III, p. 119, 1988.

[4] *A.R. Gasanov*. "Radioelectronica",1998, №6, p.75-77. (in Russian).

[5] *A.M. Pashaev, A.R. Gasanov, and Kh.I. Gasanov*. "Radiotekhnica", 1998, №2, p. 47-49. (in Russian).

[6] *A.R. Gasanov*. "Radioelectronica",1998, №12, p. 37-43. (in Russian).

[7] *A.R. Gasanov*. "Radioelectronica", 2000, №7, p.68-74. (in Russian).

[8] *A.M. Pashaev, A.R. Gasanov*. "Radiotekhnica", 1997, 7, p. 31-33. (in Russian).

[9] *A.M. Pashaev, A.R. Gasanov*. "Radiotekhnica", 1996, №8, p. 28-31. (in Russian).

A.R. Həsənov

FOTOELASTİK EFFEKTİN XASSƏLƏRİ VƏ ONLARIN TƏTBİQİ HAQQINDA BİR SIRA TƏKLİFLƏR

Bir sıra radioelektronika məsələlərinin həlli kontekstində, fotoelastik mühitlərdə akustooptik qarşılıqlı təsirin xüsusiyyətlərinin analizi verilir.

А.Р. Гасанов

ОСОБЕННОСТИ ФОТОУПРУГОГО ЭФФЕКТА И НЕКОТОРЫЕ ПРЕДЛОЖЕНИЯ ПО ИХ ПРИМЕНЕНИЮ

Анализируются особенности акустооптического взаимодействия в фотоупругих средах, в контексте их применимости для решения некоторых радиоэлектронных задач.

Received: 16.01.02

THE MODELING OF THE TWO-DIMENSIONAL POTENTIAL IN THE CHARGE-COUPLED DEVICE -STRUCTURES

E.S. MAMEDOV
Azerbaijan Technical University,
H. Javid ave. 25, Baku, Azerbaijan

The modeling of charge –coupled device (CCD)-structures in the approximation of the electrostatic potential, allowing to optimize their parameters and to reduce terms of the device projection on their base, has been carried out.

By projecting a topology it is possible to achieve functional peculiarities of CCD elements: for example, narrowing of the transfer channel by the stop-region increases the sensibility, and the complicated configuration of the shutter allows to increase the drift field [1].

Therefore, it is expedient to use the modeling for the projection of CCD-structures, which allows to optimize their parameters and to shorten terms of the device mocking up [2]. So, in the matrix photosensitive CCD (PCCD) with the element number ~10^6 the choice of alloying parameters and the structure topology provide the storage and the directed charge transfer only at the expense of two-dimensional effects [3]. The use of the quick thermal treatment for gettering of PCCD [4] allowed to increase the efficiency of the signal transfer.

The volume character of current processes causes the necessity of the corresponding modeling [5]. In spite of the fact, that CCD are devices of a dynamic type, higher values of the accumulation time in comparison with the transfer time and thermogeneration of the parasitic charge allow to use for CCD-structure modeling the Poisson and Laplace equations for the electrostatic potential provided, that the currents through p-n junctions are zero [6]. The modification of this two-dimensional model presented below takes into account the specific peculiarities of CCD-structures and allows to carry out the analysis of the potential diagrams and charge capacities of devices with complicated topologies.

The potential distribution on each work step of the CCD may be assumed as quasi-static and described by Poisson equation with standard boundary conditions [7].

The main task is the algorithm choice for the equation solution with the regard of CCD specification. The reference analysis shows, that in modern CCD, characterized by complicated impurity profiles, for the calculation of charge capacities it is necessary to consider the mobile charge carriers [8]. By this it is considered, that in the quasi-static regime of work the current in CCD-cell is absent, what allows to choose the values of quasi- Fermi levels φ_n and φ_p locally-constant. The change of the quasi- Fermi level from one constant value to another under the condition of zero current is possible in those structures regions, where concentrations of the mobile charge carrier are close to zero [9].

The depletion layers of *p–n* junctions are such regions. Therefore, region boundaries in which the constant values of quasi- Fermi levels are localized, must penetrate the depletion layers.

The depletion voltage has been determined from the relationship:

$$V_d = \varphi_d + V_c , \qquad (1)$$

where φ_d is the potential of the channel depletion, V_c is the contact potential between the ohmic-contact and a channel.

The depletion potential φ_d has been determined from the two-dimensional potential distribution in the structure by application of the voltage channel to the *p–n* junction, which is more, than the depletion voltage, but V_c value has been calculated from the potential distribution in the potential well filling:

$$Vc = \varphi_{max} - V_\alpha , \qquad (2)$$

where φ_{max} is the maximum potential in the channel at the presence of the charge, V_α is the voltage, applied to the channel at the filled well.

One of the main characteristics of CCD potential diagram is a value of potential barrier between potential wells, which gives the information about the charge transfer.

The calculation of potential barriers has been carried out on the base of the hydraulic model, according to which filling of potential wells by charge occurs analogously to the capacities filling by the fluid. The algorithm of the barrier search is as follows. The local potential maxims, which are the bottoms of the potential wells have been determined in the modeling region W. The well filling begins with the deepest one, having the maximum potential, then the next wells are consequently filled. The values of φ_k potential, at which the wells regions W_i and W_j, filled up to this level, will close up, will be the point potential of the minimal potential barrier φ_{ij} between them. The potential barriers for the junction from the potential well W_i to the well W_j have been obtained by subtraction of φ_k value from maximal potentials of wells $\varphi_{max\,i}$ and $\varphi_{max\,j}$ and vice versa.

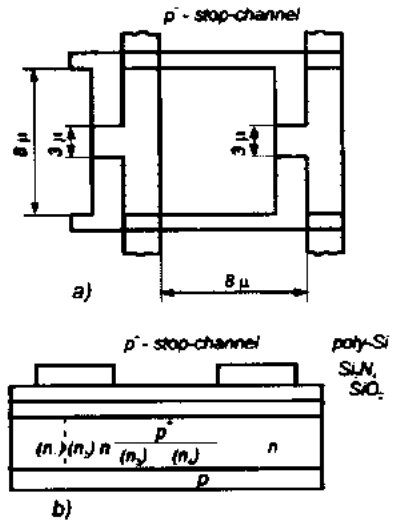

Fig.1. The topology (a) and the structure (b) of the CCD-cell with the virtual phase.

The described mathematical model and the calculation algorithm of electric characteristics are the further development of the BRK2D program, outlined in [10].

The topology of the CCD-cell is presented on fig. 1.a, peculiarity of which is the creation of the potential controllable barrier n_2 between the region of the controllable well n_1 and regions of the "virtual" well n_3 and the "virtual" barrier n_4 (fig.1.b).

For the analysis of the potential diagram of such structure at the charge transfer along the channel the algorithm of the potential reduction law in the narrow channel region by means of the shutter splitting into 2 parts has been worked out. The shutter, lying above the region of the "controllable" potential well n_1, will have the given voltage V_g, but to the shutter part, lying above the region of the "controllable" barrier n_2, will be applied some effective shutter voltage V^*_g, which is less than the real shutter voltage for the potential reduction in the channel (fig.2).

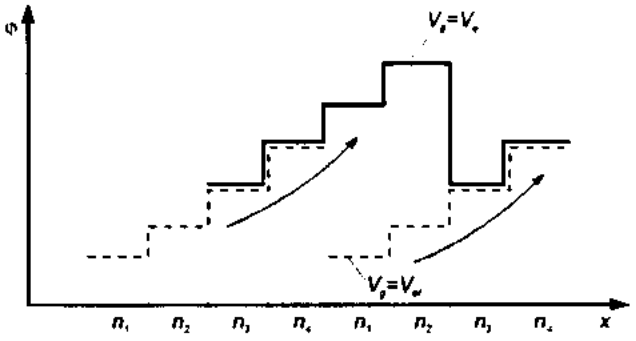

Fig.2. The potential diagram of the CCD-cell.

The algorithm of the automatic projection of the impurity profile consists of six main stages, on each of which the dose of the channel region alloying or one of the phase voltage is determined.

The voltage V_1 and alloying dose of the "controllable" well D_{n1} provided, that the surface potential barrier conservation are determined on the first stage, and dependences of the charge capacity on the voltage on the phase electrode are also calculated. On the second stage the effective shutter voltage V^*_g is determined . The phase voltage and alloying dose of D_{n2} barrier provided, that barrier retention between the filled "controllable" well and "virtual" well (near 0,5V) and the weak inversion on the interface Si-SiO_2 is determined on the third stage. The alloying dose of the virtual shutter D_p is chosen on the forth stage, and the alloying dose of the virtual barrier D_{n4} on the condition, that the barrier retention between the "controllable" and "virtual" wells are chosen on the fifth stage. The alloying dose of the "virtual" well D_{n3} at the condition of the charge transfer in the region of the "controllable" well through the "virtual" barrier is chosen on the sixth stage.

The final check of the choice correctness of the given dose is realized by the criteria of the breakdown absence in the p-n junction of the "virtual" shutter-channel and the approximate equality of the charge capacities of the "virtual" and "controllable" regions.

If the last two conditions are not fulfilled, then it is necessary to reduce the alloying dose of the "virtual" well region.

The similar algorithm of the projection was applied earlier for the optimization of the photodiode CCD-element [11].

The distribution profiles of the mobile charge for different time intervals, calculated for the structure with the shutter length L=4 mcm, with concentration of the alloyed impurity in the substrate N_D= 10^{15}cm^{-3}, with the oxide thickness d=0.2 mcm, with the gap width between shutters 200 nm, has been shown on fig.3. It is seen, that the drift fields determine the process of the charge transfer after 800 ps, and the influence of self-inducted drift becomes negligibly small.

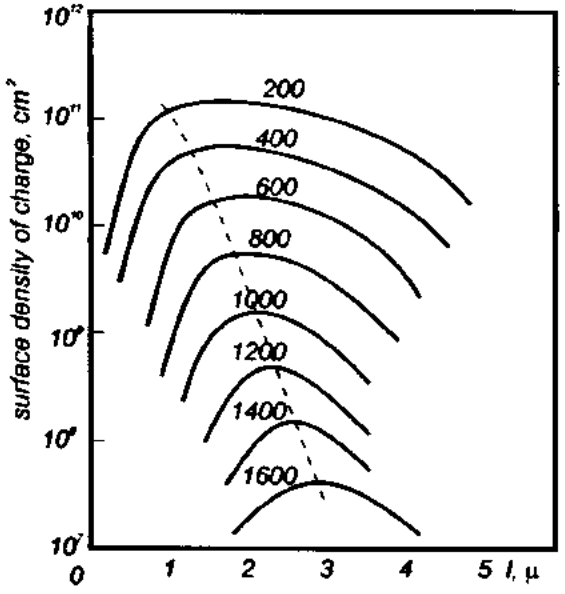

Fig.3. Profiles of the charge distribution under the transfer electrode for different time moments (ps)

The charge profile moves to the right with the time increase, i.e to the accumulation side, however instead of the constant shift after 1400ps the form of the charge distribution stabilizes.

The reason of this is in the large drift fields, accelerated by the carriers near boundaries between the transfer electrode and the accrual electrode.

Hence, on the initial stage of the charge transfer the self-inducted drift may be the main reason of the carriers motion at the large charge densities, however during 1ns the influence of the thermal diffusion and drift fields will determine the final part of the charge transfer process.

Consequently, if even 99% of the charge may be carried by the influence of the self-inducted drift, the thermal diffusion and the drift field, which at the absence of carriers capture may provide the indicated efficiency of the transfer for some nanoseconds, play the important part for the achievement of the transfer efficiency 99,99% (i.e. the transfer inefficiency ε=10^{-4}). In the absence of drift fields the final stage of the transfer process is determined by the thermal diffusion and characteristic times increase to some hundreds of nanoseconds.

The reason of this is in the large drift fields, accelerated by the carriers near boundaries between the transfer electrode and the accumulation electrode.

Hence, on the initial stage of the charge transfer the self-inducted drift may be the main reason of the carriers motion at the large charge densities, however during 1ns the

influence of the thermal diffusion and drift fields will determine the final part of the charge transfer process.

Consequently, if even 99% of the charge may be carried by the influence of the self-inducted drift, the thermal diffusion and the drift field, which at the absence of carriers capture may provide the indicated efficiency of the transfer for some nanoseconds, play the important part for the achievement of the transfer efficiency 99.99% (i.e. the transfer inefficiency $\varepsilon = 10^{-4}$). In the absence of drift fields the final stage of the transfer process is determined by the thermal diffusion and characteristic times increase to some hundreds of nanoseconds.

[1] *J. Hynecek.* Design and performance of a high-resolution image sensor for color TV applications. IEEE Trans. on Electron Devices, 1985, ED-32, №8, p. 1421-1429.

[2] *H.S. Wong, Y.L. Yao, E.S. Schling.* IBM J. Res. Develop., 1992, v.36, №1, p. 83-106.

[3] *E.G.Stevens, B.C. Burkey, D.W. Nichols.* A 1-megapixel, progressive-scan image sensor with antiblooming control and lag-free operation. IEEE Trans. on Electron Devices, 1991, ED-38, №5, p. 981-987.

[4] *F.D. Kasimov, E.S. Mamedov.* "METD"-2001, Baku, Sumgait, 2001, p. 83-84.

[5] *V.I. Khainovskii, V.V. Uzdovskii, N.M. Gordo.* Izvestiya Vuzov. Electronica, 2000, №1, p. 28-35.

[6] *J.A. Greenfield, R.W. Dutton.* IEEE Trans. on Electron Devices, 1980, ED-27, №6, p. 1520-1432.

[7] *A.A. Pugachev.* The program provision for the calculation of MIS and CCD LSI elements characteristics in the low current regime- The abstracts of Republic conference reports: " Numerical methods and projection means and the elements testing of the solid-state electronics. Tallinn, 1989, p. 78

[8] *K. Hwang, D. Navon.* IEEE Trans. on Electron Devices, 1984, ED-31, №9, p. 1126-1135.

[9] *A.I. Kanunnikov, A.A. Pugachev, S.S. Tataurschikov.* The modeling and optimization of structural technological characteristics of CCD- structures -The thesis of 4-th Conference reports with the International participation "Charge-coupled devices and systems on their base", Gelendjik-Moscow, 1992, p. 152.

[10] *K.O. Petrosyants, A.A. Pugachev.* Radioelectronica, 1989, №6, p.78-81.

[11] *A.A. Pugachev, Y.I. Tischin, A.I. Kanunnikov, S.B. Kuzmin.* " The calculation and optimization of the photodiode CCD-element with low sizes. The abstracts of the 4-th conference reports with the International participation "Charge-coupled devices and systems on their base". Gelendjik-Moscow, 1992, p. 15-16.

E.S. Məmmədov

YƏC-STRUKTURLARDA İKİÖLÇÜLÜ POTENSİALLARIN MODELLƏŞDİRİLMƏSİ

Elektrostatik potensiallar yaxınlaşmasında YƏC-strukturların modelləşdirilməsi aparılmışdır, bu da ki, onların parametrlərini optimallaşdırmağa və onlar əsasında cihazların layihələndirmə müddətlərini azaltmağa imkan verir.

Э.С. Мамедов

МОДЕЛИРОВАНИЕ ДВУМЕРНОГО ПОТЕНЦИАЛА В ПЗС-СТРУКТУРАХ

Проведено моделирование ПЗС-структур в приближении электростатического потенциала, позволяющее оптимизировать их параметры и сократить сроки проектирования приборов на их основе.

Received: 16.01.02

THERMOSTIMULATED CONDUCTIVITY IN $ZnGa_2Se_4$

A.G. SULTANOVA

Institute of Physics of the Azerbaijan National Academy of Sciences
H. Javid av. 33. Baku. 370143

Thermostimulated conductivity and trap levels were investigated in $ZnGa_2Se_4$ monocrystals. It was shown that the quick recombination mechanism is realized in $ZnGa_2Se_4$ monocrystals.

Tetragonal compounds with the common chemical $A^2B_2^3C_4^6$ formula attract an attention owing to their perspective for use in semiconductor devices. These compounds are characterized by the high photosensitivity, dazzling luminescence, weak dependence of their properties on external factors, high stability of time characteristics. Moreover, complex chemical composition, presence of two types atoms in cation sublattice form a rich spectrum of the local centers in the gap band. However, their nature and energy spectra in fact have not been investigated. That is why, complex investigation of their physical properties is actual.

It is known that the method of thermostimulated conductivity (TC) is widely used for definition of the recombination mechanism, spectrum of local states and parameters of traps in wide-band semiconductors. In spite of some works [1-4] dedicated to investigation of optical spectra of $ZnGa_2Se_4$, spectra of local states in practice have not been investigated. There is only one work [5] which presents results of TC in $ZnGa_2Se_4$. Authors of the work [5] observed the TC maximum at 120K with the broadened edge in the high temperature range and supposed that trap centers are distributed quasicontinuously.

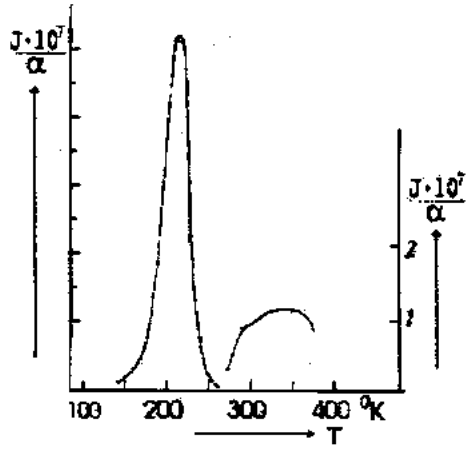

Fig. 1. Spectrum of the thermostimulated conductivity in $ZnGa_2Se_4$.

In this paper the results of TC investigation in $ZnGa_2Se_4$ are presented with the purpose of determination of the spectrum of local states and the recombination mechanism.

For realization of TC measurements the monocrystalline samples of $ZnGa_2Se_4$ were obtained by the gas transport reactions method. The crystal of iodine was used as a transporter. Lattice parameters a=5.496Å, c=10.99Å, c/a=2 were determined by the X- ray method.

In the fig.1 the TC spectrum of $ZnGa_2Se_4$ is represented. In TC spectrum the maximum at 219K and wide line in the interval 240÷400K with the maximum at 346K is observed.

In common case for clearing up of the recombination mechanism relationships $\delta' = T_M - T_1$ and $\delta'' = T_2 - T_M$ are used, where T_M is the temperature at the maximum of TC, T_1 and T_2 are temperatures where the conductivity reaches half of its value on growing and falling down wings of the TC maximum [6]. In the case, when the condition $\delta > \delta''$ is fulfilled , the quick mechanism of recombination is realized, if $\delta' < \delta''$ then the slow mechanism is realized and in case $\delta' = \delta''$- the mixed mechanism of recombination is fulfilled. In the case of the quick mechanism of recombination, when the quasiequilibrium exists between trap levels and conduction band, the condition is performed

$$\delta \geq e^{-1}(1+2kTm/E_1) \qquad (1)$$

where $\delta = (T_2 - T_M)/(T_2 - T_1)$, E_1 is the depth of the trap levels. Analysis of the TC maximum at 219K showed that conditions $\delta' > \delta''$ are performed, that is the quick mechanism of recombination exists in $ZnGa_2Se_4$. Therefore by use of the formula (1) we estimated the depth of trap levels as 0.24 eV.

Presence of the wide TC maximum in the range 240÷400 K with the maximum of 346 K testifies that the gap band in $ZnGa_2Se_4$ has a few near disposed trap levels in this range of temperature.

[1] *I.A. Beun, R. Nitsche, M. Sichensteiler.* Physic, 1961, v.27, №3, p. 448-452.

[2] *Whe-Tek Kim, Chang-Sub Chung, long-Geum Kim, Moon-Seig Jin Hyung-Gon Kim.* Phys. Rev. B., 1988, v.38, №3, p. 2166-2168.

[3] *Yong-Geun Kim, Wha-Tek Kim, Jin Sup Kim, Dong Sung Ma, Hong-Lee Park.* Phys. Rev. B., 1989, v.39, №12, p. 8747-8749.

[4] *M.Turowski, A. Kisiel.* J. Phys. C., Solid State Phys., 1984, v.17, №25, p. 1661-1664.

[5] *S.J. Radautsan, J.M. Tigiryanu, V.N. Fulga, Yu.O. Derid.* Phys. Stat. Sol. (a), 1989, 114, p. 259-263.

[6] *K.H. Nicolas, J. Woods.* Brit.J. Appl. Phys., 1964, v.15, №7,p. 783-785.

A.G. SULTANOVA

A.Q. Sultanova

$ZnGa_2Se_4$ MONOKRİSTALLARINDA TERMOSTİMULƏ KEÇİRİCİLİYİ

$ZnGa_2Se_4$ monokristallarında termostimulə keçiriciliyi (TSK) tədqiq olunmuşdur və tələ səviyyələri təyin edilmişdir. Göstərilmişdir ki, $ZnGa_2Se_4$ monokristallarında sürətli rekombinasiya mexanizmi realizə edilir.

А.Г. Султанова

ТЕРМОСТИМУЛИРОВАННАЯ ПРОВОДИМОСТЬ В $ZnGa_2Se_4$

Исследованы спектры термостимулированной проводимости монокристаллов $ZnGa_2Se_4$. Определены глубина залегания ловушечных уровней. Показано, что в $ZnGa_2Se_4$ реализуется быстрый механизм рекомбинации.

Received: 11.02.02

CONFORMATIONAL STUDY OF THE *N*-TERMINAL PENTAPEPTIDE FROM GUANYLYL CYCLASE *A*

N.T. SULEYMANOVA, I.N. ALIEVA, D.I. ALIEV, N.M. GODJAYEV
Baku State University
Z. Khalilov str.23, Baku, 370148

The conformational peculiarities of the Arg-Thr-Tyr-Trp-Leu *N*-terminal pentapeptide from catalytic domain of the guanylyl cyclase *A*, the atrial natriuretic peptide receptor have been investigated by theoretical conformational analysis method. The energy and geometrical parameters corresponding to the optimal conformers of the fragment are obtained.

INTRODUCTION

Guanylyl cyclase (GC-*A*) is the receptor for the atrial natriuretic peptide (ANP) [1-3]. ANP binding to GC-*A* has been demonstrated by both ligand binding analysis and affinity cross-linking studies [4,5]. ANP directly activates GC-A purified from mammalian tissues and increases cGMP level in a concentration- and time- depended fashion in a variety of cells [6-9].

The deduced primary sequences of the natriuretic peptide receptors predicted a protein with a single transmembrane domain that divides an extracellular ligand- binding domain from an intracellular domain. Deletion mutagenesis studies have demonstrated that the intracellular domain serves regulatory, dimerization, and catalytic functions [6]. This regulatory domain has sequence similarity with protein kinases, particularly the protein tyrosine kinases, which are also single transmembrane domain receptors [10]. The sequences of the *C* - terminal catalytic domains are highly homologous to those of the α - and β - subunits of soluble GC (sGC) and have limited identity with the two catalytic domains of adenylyl cyclase [11]. We report here on the conformational study of the Arg-Thr-Tyr-Trp-Leu *N*-terminal pentapeptide fragment from catalytic domains of the GC-*A*. A molecular model and calculation scheme are illustrated in Figure 1.

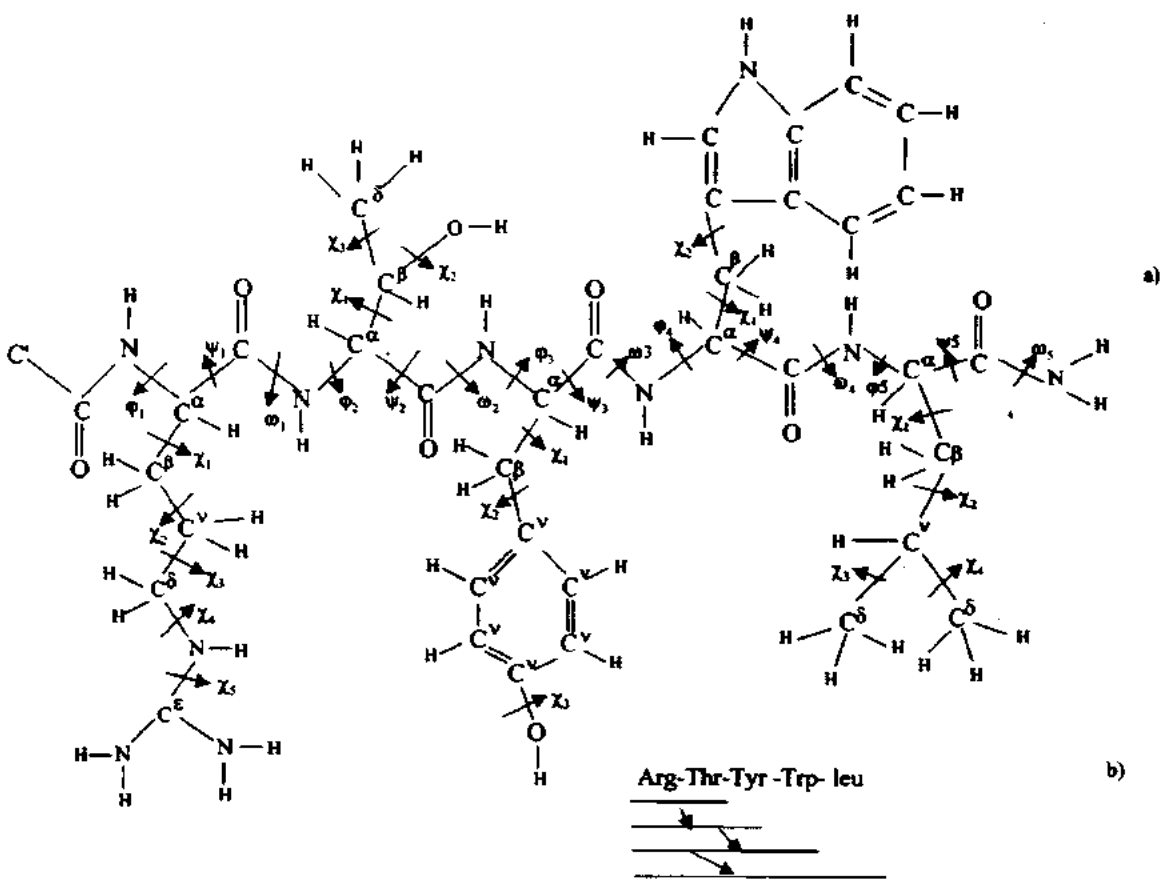

Fig.1. A molecular model (a) and calculation scheme (b) of pentapeptide from catalytic domain.

METHOD AND MODEL FOR CALCULATION

Theoretical conformational analysis was used to study the low-energy conformations available to *N*-terminal pentapeptide fragment of the GC-A. The calculations were carried out on the basis of the approach as described in Ref [12]. The conformational potential energy is considered as the sum of independent contributions of nonbonded (E_m), electrostatic (E_q), torsional (E_{tor}) interactions and intramolecular hydrogen

bonding energies (E_{nb}).The energy of nonbonded interactions has been described by Lennard-Jones potential with the parameters proposed by Momany et.al. [13]. A contribution of electrostatic interactions has been taken into account in a monopole approximation according to Coulomb's law, with partial charges of atoms as described in Ref [14]. The effective dielectric constant was taken as equal to ten as described by Lipkind et.al. [14]. The intrinsic energy of a molecule includes also the torsion potentials, describing the barriers of the inner rotation between atoms that have a 1-4 relationship, the values of the torsional barriers heights are taken from work [13]. The energy of hydrogen bond formation is calculated based on Morse potential [13] and dissociation energy of hydrogen bond is taken to be -1,5 kcal·mol^{-1} at an NH... OC distance r0=1.8 Å.

The bond distances and the values of valence angles were regarded as invariable and correspond to [13]. Only dihedral angles were taken to be the intrinsic degrees of freedom. The conventions used for rotational angles correspond to the IUPAC-IUB nomenclature [15]. The identifier system will be used to describe all structures at the intermediate stages of the calculation experiment, with the numerical values of geometry parameters produced only at the final stage. *B, R, L* and *P* symbols were used to represent the regions of conformational space situated around φ, ψ values as following: $R(\varphi, \psi$=-180-0°), $B(\varphi$=-180-0°, ψ=0-180°), $L(\varphi, \psi$=0-180°) and $P(\varphi$=0-180°, ψ=-180-0°).

The backbone is conventionally described by the "shape" symbols e and f referred to as respectively the extended and folded configuration of peptide chain. Pentapeptide stable conformations were found by the total conformational energy minimization. The minimization procedure has several steps. A final conformation obtained in a preliminary optimization step is taken as an initial one for the next step. A procedure for the pentapeptide global energy was repeated until the minimal values of the global energy retained constant level. Based on the above considerations and calculation program [16] the detailed conformational analysis of the Arg-Thr-Tyr-Trp-Leu pentapeptide was carried out.

RESULTS AND DISCUSSION

According to the calculation scheme (fig.1) the conformations of consequently lengthened di-, tri-, tetra-and finally pentapeptide fragment were calculated (due to ref.[12] the final results are independent on the way of the peptide backbone dividing into fragments). The initial conformations for the pentapeptide energy minimization were obtained by combining the of lowest energy structures of Arg, Thr, Tyr, Trp, and Leu amino acid residues. Initial monopeptide conformations are chosen as given in Ref. [12]. The backbone chains of the amino acid residues, that construct the pentapeptide, can be in *R, B* and *L*- forms. The side chain dihedral angle values χ_1=±60 and 180° were taken into account for threonine, tyrosine and tryptohan.

For *N*- terminal of the fragments, however only χ_1=60 and 180° and for the *C*-terminal only χ_1=60 and –60° were considered. Since the variation of χ_2 angle of the threonine has not altered the conformational energy significantly, only one of the equal probably conformations (χ_2=±60, 180°), i.e. χ= 180^0 was taken into account for this residue. For tyrosine, the value of 90° for χ_2 and 180° for χ_3, which correspond to stable states, were used. Thus, for the first approach to Arg-Thr-Tyr-Trp-Leu pentapeptide 24 low-energetic conformers of Arg and 9 rotomers of Leu, Thr, Tyr, Trp were considered. The pentapeptide fragment involves 108 atoms and 33 dihedral angles as indicated in fig 1. All available conformations were classified into 16 shapes. About 324 initial conformations were used for the global energy minimization. Only six of them consist of low energy conformers the relative energy of which is within 0-5kcal·mol^{-1}.

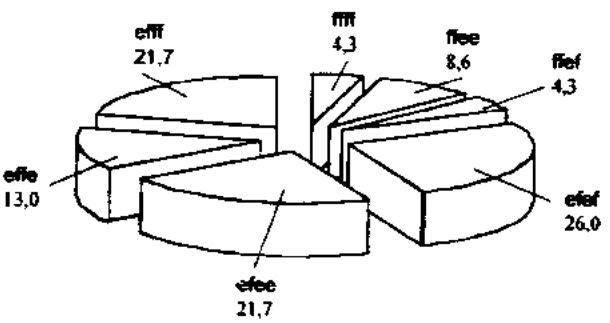

Fig.2. The low-energetical conformations distribution (in percent) for the pentapeptide favourable shapes within E_{nb}=0÷5kcal·mol^{-1}.

The energy distribution of the shapes is illustrated in fig.2. Several helical structures with the folded backbone shape, including the α- helix (RRRR shape), are the most preferred one.

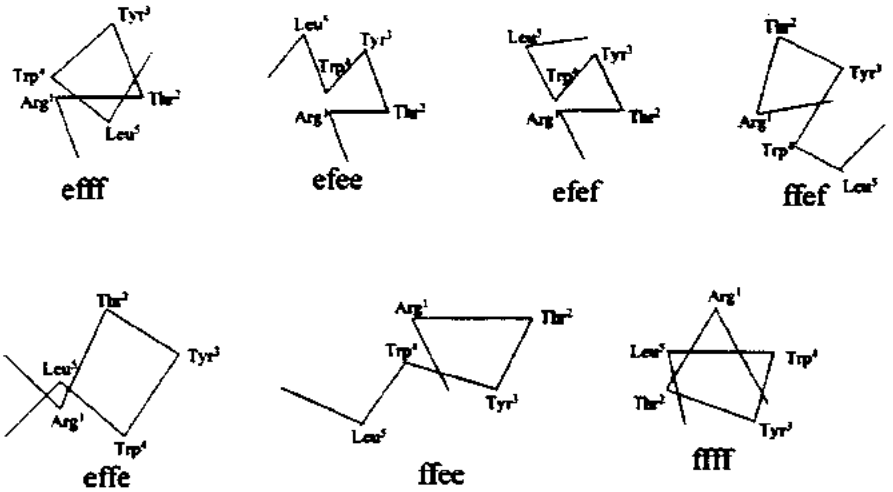

Fig. 3. The schematic representations of the shapes of the low energetical conformations of pentapeptide, based on the coordinates of C^{α} atoms.

Table 1. The energies (kcal· mol^{-1}) and shapes of favourable conformations of the Arg-Thr-Tyr-Trp-Leu fragment

№	SHAPE	Conformation	Inter residue interaction energies										Energy contribution			E_o
			Arg Thr	Thr Tyr	Tyr Trp	Trp Leu	Arg Tyr	Thr Trp	Tyr Leu	Arg Trp	Thr Leu	Arg Leu	E_{nb}	E_{el}	E_{tor}	
1	efff	BRRRB	-1.71	-2.93	-1.18	-3.49	-5.39	-0.45	-0.62	-4.88	-0.90	-2.31	-26.9	2.1	1.4	0.0
2	efee	BRRLB	-1.90	-1.14	-1.55	-0.61	-5.58	-2.94	-4.99	-4.11	-0.16	-0.09	-28.9	2.7	3.0	1.2
3	efef	BRBRR	-1.94	-0.95	-4.41	-1.05	-2.79	-1.19	-2.54	-7.64	0.00	-0.58	-27.7	3.6	4.2	3.6
4	ffef	RRBRR	-2.41	-2.43	-2.48	-4.62	-1.34	-0.20	-2.00	-0.24	-0.01	-0.03	-25.8	4.9	1.6	4.2
5	ffee	RRBBR	-2.44	-1.83	-2.61	-3.50	-1.39	-0.20	-2.82	-0.22	0.00	-0.02	-25.5	4.8	1.6	4.2
6	effe	BRBLR	-1.48	-0.55	-1.67	-3.11	-7.42	-0.30	-1.60	-5.85	-1.28	-1.71	-25.5	3.2	3.6	4.7
7	ffff	RRRRR	-2.66	-1.12	-1.92	-5.25	-1.73	-1.03	-0.54	-1.60	-0.62	-3.11	-28.2	5.6	4.1	4.9

Table 2. The geometrical parameters (in degree) of the pentapeptide fragment for low-energetical conformations

Amino Acid	CONFORMATIONS*						
	1	2	3	4	5	6	7
Arg	φ=-118 ψ=120 ω=179 χ_1=181 χ_2=177 χ_3=178 χ_4=179 χ_5=179	φ=-118 ψ=137 ω=179 χ_1=182 χ_2=176 χ_3=179 χ_4=179 χ_5=170	φ=-144 ψ=157 ω=179 χ_1=60 χ_2=178 χ_3=183 χ_4=179 χ_5=180	φ=-91 ψ=-55 ω=179 χ_1=179 χ_2=177 χ_3=179 χ_4=179 χ_5=179	φ=-94 ψ=-53 ω=180 χ_1=179 χ_2=178 χ_3=179 χ_4=179 χ_5=179	φ=-140 ψ=159 ω=179 χ_1=55 χ_2=176 χ_3=181 χ_4=179 χ_5=179	φ=-109 ψ=-58 ω=180 χ_1=178 χ_2=177 χ_3=179 χ_4=179 χ_5=179
Thr	φ=-86 ψ=-52 ω=178 χ_1=56 χ_2=180 χ_3=176	φ=-101 ψ=-68 ω=179 χ_1=57 χ_2=180 χ_3=175	φ=-93 ψ=-57 ω=177 χ_1=57 χ_2=180 χ_3=175	φ=-86 ψ=-60 ω=178 χ_1=57 χ_2=180 χ_3=173	φ=-87 ψ=-56 ω=181 χ_1=57 χ_2=180 χ_3=173	φ=-85 ψ=-30 ω=185 χ_1=195 χ_2=181 χ_3=176	φ=-76 ψ=-45 ω=185 χ_1=57 χ_2=180 χ_3=174
Tyr	φ=-141 ψ=-60 ω=179 χ_1=-59 χ_2=90 χ_3=179	φ=-140 ψ=-69 ω=170 χ_1=168 χ_2=71 χ_3=170	φ=177 ψ=-108 ω=177 χ_1=188 χ_2=84 χ_3=179	φ=-127 ψ=164 ω=174 χ_1=58 χ_2=84 χ_3=179	φ=-122 ψ=171 ω=175 χ_1=66 χ_2=87 χ_3=179	φ=-105 ψ=160 ω=193 χ_1=65 χ_2=84 χ_3=179	φ=-80 ψ=-21 ω=184 χ_1=64 χ_2=81 χ_3=179
Trp	φ=-100 ψ=-63 ω=180 χ_1=189 χ_2=195	φ=43 ψ=57 ω=168 χ_1=-57 χ_2=130	φ=-68 ψ=-61 ω=194 χ_1=-56 χ_2=167	φ=-94 ψ=-56 ω=178 χ_1=175 χ_2=-132	φ=-139 ψ=141 ω=178 χ_1=177 χ_2=-121	φ=53 ψ=69 ω=177 χ_1=186 χ_2=188	φ=-92 ψ=-59 ω=185 χ_1=176 χ_2=-146
Leu	φ=-119 ψ=140 ω=181 χ_1=-59 χ_2=179 χ_3=180 χ_4=179	φ=-125 ψ=113 ω=178 χ_1=192 χ_2=189 χ_3=180 χ_4=179	φ=-100 ψ=-72 ω=185 χ_1=171 χ_2=192 χ_3=180 χ_4=179	φ=-98 ψ=-58 ω=180 χ_1=179 χ_2=184 χ_3=180 χ_4=179	φ=-103 ψ=-59 ω=179 χ_1=177 χ_2=185 χ_3=180 χ_4=178	φ=-100 ψ=-59 ω=179 χ_1=-60 χ_2=180 χ_3=180 χ_4=179	φ=-97 ψ=-66 ω=188 χ_1=-179 χ_2=182 χ_3=180 χ_4=179
E_{rel}·kcal· mol^{-1}	0.0	1.2	3.6	4.2	4.3	4.7	4.9

* Conformation numbering is the same as given in Table 1.

The lowest energy conformer, namely the global conformer of the pentapeptide has efff shape. The large side chains of terminal residues in all helical- types conformers approach to each other and form effective tetra-and pentapeptide interactions (Table 1). The stable structures of the two shapes ffff and efff form a hydrogen bond NH(Leu)...OC (Arg). Specific interaction between the pairs of the Trp and Leu residues (-4.4 kcal-mol.$^{-1}$ in average) also made an important contribution to the stabilization of these conformations. It is found that the strong interaction between Arg and Trp (- 6.2 kcal· mol $^{-1}$, in average) is characteristic for all low energy structures of the pentapeptide from the efff, efef, efee and

effe shapes. As seen in Table 1, both Tyr and Trp make an important contribution towards the dispersion interactions to the stabilization of the low-energetic structures of the pentapeptide from efef shape (~4.4kcal·mol^{-1}) The geometrical parameters of low-energetical conformations are given in Table 2. In figure 3, the main chain shapes of the pentapeptide corresponding to the low- energetical conformations are illustrated.

[1] *K.A. Lucas, G.M. Pitari, Sh. Kazerounian, I. Ruiz-Stewart, J. Park, S. Schulz, K.P. Chepenik, S.A. Waldman.* "Guanylyl Cyclases and Signaling by cyclic GMP", Pharmacol. Rev., 2000, v. 52, p. 375-413.

[2] *B.J. Wedel, D.C. Foster, D.E. Miller, D.L. Garbers.* Proc. Natl. Acad. Sci. USA, 1997, v. 94, p. 459-462.

[3] *D.K. Thompson, D.L. Garbers.* J. Biol. Chem., 1995, v. 270, p. 425-430.

[4] *Jr. Jewett, K.J. Koller, D.V. Goeddel, D.G. Lowe.* EMBO J., 1993, v. 12, p. 769-777.

[5] *D.G. Lowe, M.S. Chang, R. Hellmiss, E. Chen, S. Singh, D.L. Garbers, D.V. Geoddel.* EMBO J., 1989, v. 8, p. 1377-1384.

[6] *M. Chinkers, D.L. Garbers, M.S. Chang, D.G. Lowe, H.M. Chin, D.V. Goeddel, S., Schulz.* "A membrane form of guanylate cyclase is an atrial natriuretic peptide receptor" Nature (Lond), 1989, v. 338, p. 78-83.

[7] *S.K. Wong, C.P. Ma, D.C. Foster, A.Y. Chen, D.L. Garbers.* J. Biol. Chem., 1995, v. 270, p.30818-30822.

[8] *T.Inagami, R.Takayanagi, R.M.Snajdar.* Methods Enzymol., 1991, v. 195, p.404-413.

[9] *S.A. Waldman, D.C. Leitman, F. Murad.* Methods Enzymol., 1991, v.195, p.397-404.

[10] *S. Singh, D. G.Lowe, D.S. Thorpe, H. Rodriguez, W.J.Kuang, L.J. Dangott, M. Chinkers, D.V. Goeddel D.L. Garbers.* "Membrane guanylate cyclase is a cell-surface receptor with homology to protein kinases" Nature (Lond), 1988, v.334, p.708-712.

[11] *D.S. Thorpe and D.L. Garbers.* J. Biol. Chem., 1989, v. 264, p. 6545-6549.

[12] *E.M. Popov.* Int. J. Quant. Chem., 1979, v. 16, p.707-737.

[13] *F.A. Momany, R. M$_c$ Guire, A.W.Burgess, H.A Scheraga.* J. Phys. Chem .1975, v. 79, 2361-2381.

[14] *G.M. Lipkind, S.F. Arkhipova, E.M. Popov.* Int. J. Pept. Prot. Res., 1973, v. 5, p. 381-397.

[15] *I.S. Maksumov, L.I. Ismailova, N.M. Godjaev.* J. Struc. Chem., 1983, v. 24, No. 4, p. 147-148. (in Russian).

[16] IUPAC- IUB Commision on Biochemical Nomenclature Abbreviations and symbols for Description of conformation of polypeptide chains,Pure Appl. Chem., 1974, v. 40, p. 291-308.

N.T. Süleymanova, İ.N. Əliyeva, C.İ. Əliyev, N.M. Qocayev

QUANİLATSUKLAZA *A* PENTAPEPTİDİNİN *N*-SONLUQLU KONFORMASİYA ANALİZİ

Nəzəri konformasiya analizi metodu ilə natriuretik peptidin reseptoru quanilatsiklaza *A*-Arg-Thr-Tyr-Trp-Leu katalitik domenin *N*-sonluqlu pentapeptid fraqmentinin konformasiya xüsusiyyətləri öyrənilmişdir. Fraqmentin optimal konformasiya vəziyyətlərinin enerji və həndəsi parametrləri alınmışdır.

Н.Т. Сулейманова, И.Н. Алиева, Д.И. Алиев, Н.М. Годжаев

КОНФОРМАЦИОННЫЙ АНАЛИЗ *N*-КОНЦЕВОГО ПЕНТАПЕПТИДА ГУАНИЛАТЦИКЛАЗЫ *A*

Методом теоретического конформационного анализа изучены конформационные свойства N-концевого пентапептидного фрагмента Arg-Thr-Tyr-Trp-Leu каталитического домена гуанилатциклазы *A*-рецептора предсердного натрийуретического пептида. Установлены энергетические и геометрические параметры оптимальных конформационных состояний фрагмента.

Received: 01.03.02

THE EQUATION FOR LIQUIDUS LINE OF THE In_2Te_3-Co_3Te_4 SYSTEM PHASE DIAGRAM

Ch. ABILOV, C.A. ZEYNALOV
Azerbaijan Technical University
H. Javid ave.25, Baku

The equation for a calculation of the liquidus line of the In_2Te_3-Co_3Te_4 system state diagram was derived. With this purpose, the liquidus line, consisting of two branches, was accepted to be similar to branches of two parabolas, that is why the parabola equation was used for the derivation of the mathematical expression. Using the suggested equation, content values and fusion temperatures of interacting components may be calculated with high accuracy, in the broad concentration interval.

The phase state diagram of the system In_2Te_3-Co_3Te_4 was earlier constructed on the base of the experimental data of the complex of physico-chemical analysis methods [1] and it was revealed, that on curves of the alloy thermogram heating, concentrated by In_2Te_3, the effects, connected with the polymorphic transformation of the ordered modification α-In_2Te_3 into the unordered β-In_2Te_3, are clearly manifested. It was also established, that the temperature of the phase transition α- In_2Te_3 into β- In_2Te_3 increases from 890 K up to 960 K under the influence of Co_3Te_4 and the dependence of the phase transition temperature on the concentration occurs here. Therefore, the confirmation of figure points coordinates of the state diagram of this system by theoretical calculations is an actual one.

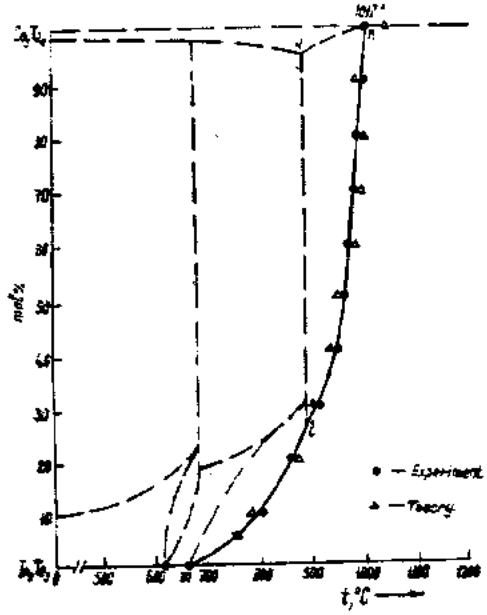

Fig.1. The part of the state diagram of the system In_2Te_3-Co_3Te_4 in the high temperature region.

There are a number of works, devoted to thermodynamic calculations of liquidus line of binary and more complicated systems. However, there is no information about mathematical calculations. The authors of [2] made an attempt to receive the restriction equation for the calculation of binodile stratification curves in systems Hg-Tl_2X (where X=S, Se, Te). The results of the derivation of the equation for the liquidus curve plotting and boundaries determination of the phase formation reaction in the system In_2Te_3-Co_3Te_4 are given in the present report. Main lines fragments of the phase interface of the system In_2Te_3-Co_3Te_4 are presented on fig.1. For clarity the scheme was constructed in the form of the dependence x-$f(t)$, where x is the crystal content, t is the temperature (the content is meant through U in the derived equations). The liquidus lines on the state diagram may be observed as branches of two parabolas. One branch (*nl* line) is the part of the large parabola, the other (*ml* line) is the half of the smaller parabola. Therefore, analytical expressions of ordinary parabolas served the base for worked out equations of liquidus lines. The analysis of the results of the undertaken research showed, that the change of the substance transformation rate versus the temperature may be described by the following linear differential equation [3].

$$\frac{dU(t)}{dt} = (a + bt)U(t), \qquad (1)$$

where $U(t)$ describes the substance state versus the temperature, a and b are parameters, characterizing the influence of the temperature change on the substance state. It is necessary to note, that the equation (1) is observed with the initial condition:

$$U(t_0) = U_0 \qquad (2)$$

It is necessary to solve (1) with the initial condition (2) for determination of the change degree of the substance state. Let us rewrite (1) as

$$\frac{dU(t)}{U(t)} = (a + bt)dt \qquad (3)$$

and suggest, that $t_0=0$. The solution of the equation (3) with the initial condition $U(0)=U_0$ looks as:

$$bt^2 + 2at - 2\ln\left[\frac{U(t)}{U_0}\right] = 0 \qquad (4)$$

Calculating the quadratic equation (4), we obtain t as the function of U

$$t(U) = \frac{-a \pm \sqrt{a^2 + 2b\ln\left[\frac{U(t)}{U_0}\right]}}{b} \qquad (5)$$

Now if:

1. $a^2 + 2b\ln\left[\frac{U(t)}{U_0}\right] = 0$, then it follows from (5), that

$t(U) = -\frac{a}{b}$ ($a>0, b<0$), i.e. in this case $t(U) = -\frac{a}{b} = const > 0$.

2. $a^2 + 2b\ln\left[\frac{U(t)}{U_0}\right] > 0$, i.e. $a^2 > -2b\ln\left[\frac{U(t)}{U_0}\right]$, or $|a| > \sqrt{-2b\ln\left[\frac{U(t)}{U_0}\right]}$, where $b<0$. In this case the function $t(U)$ has two representations, namely:

$$t_1(U) = \frac{-a + \sqrt{a^2 + 2b\ln\left[\frac{U(t)}{U_0}\right]}}{b}$$

$$t_2(U) = \frac{-a - \sqrt{a^2 + 2b\ln\left[\frac{U(t)}{U_0}\right]}}{b} \qquad (6)$$

At all parameters values $a>0$, $b<0$ or $a<0$, $b>0$ the function (9) is positive. It is possible to apply the simple polynomial equation for determination of concrete values of "a" and "b". The most suitable method of these parameters determination is the method of the least squares. However, it is possible to use more simple method for our case, for example: the method of means. Guided by this method and having divided the liquidus line into 2 temperature intervals (the first interval spreads to ml line, the second to *nl*), we determined the "a" and "b" parameters values . In fact, on the experimentally constructed diagram of the liquidus line there is a break at the beginning of the peritectoid transformation (lk line). For the interval 667<t<917°C it has been found from the calculation of means, that a=-3·10^{-3} (degree^{-1}), b=9.7·10^{-6} (degree^{-2}). In this case, the equation (4) will take a form

$$LnU - lnU_0 = b/2t^2 + at$$

or

$$U = U_0 exp(at + b/2t^2)$$

$$U = exp(-3\cdot10^{-3}t + 4.87t^2)$$

The equation was observed with the initial conditions $U_0=U(667)=1$.(The unit reflects the initial components content, i.e In_2Te_3 without Co_3Te_4 admixture).

It was found for the temperature interva 1917<t<1017°C, that a=-2.7·10^{-2} (degree^{-1}), b=4.2·10^{-5} (degree^{-2}). Consequently, $lnU=ln$ 100-2.7·10^{-2} t+2.1·10$^{-5}t^2$, with the regard of the initial condition $U(t_0)$ =U(1017)=100, i.e. the approach start was taken from the Co_3Te_4 side).

The experimental and calculated values of fusing temperature and content of system alloys In_2Te_3-Co_3Te_4.

Table 1

Experiment		Calculation	
Content mole %	Temperature °C	Content mole %	Temperature °C
10	792	10.2	788
20	877	19.7	878
30	927	29.9	926
40	972	39.8	971
50	982	51.4	980
60	987	58.4	988
70	992	66.7	994
80	997	76.0	998
90	1007	88.6	1003
100	1017	99.0	1043

[1] S.A. Zeynalov. Research of In_2Te_3-Cr_3Te_4 (Co_3Te_4) system state diagram near In_2Te_3 compound. Reports of the Republic scientific conference of young investigators and post-graduate. Baku, MNO 1999, p. 24-25.

[2] M.M. Asadov, N.N. Jabrailov. Izv. AN SSSR: Non-organic materials. .1988. v.24. № 11. p.1923-1925.

[3] Bohr G. "Quasiperiodical functions" M., IL, 1939, p. 98.

[4] I.N. Bronshtein, K.A. Semendyaev. "The reference book on mathematics" M: " Fizmathgiz".1966.

Ç.İ. Əbilov, S.A. Zeynalov

In_2Te_3-Co_3Te_4 SİSTEMİNİN FAZA DİAQRAMININ LİKVİDUS ƏYRİSİNİN TƏNLİYİ

In_2Te_3-Co_3Te_4 sisteminin hal diaqramındakı likvidus əyrisinin nəzəri qurulması üçün riyazi tənlik müəyyənləşdirilmişdir. Bu məqsədlə, iki hissədən ibarət olan likvidus əyrisini parabolanın qolları kimi qəbul edərək, parabola təni kimi qabul edərək, parabola tənliklərindən istifadə edilmişdir. Müəyyənləşdirilən tənlikdən istifadə edərək yüksək dəqiqliklə geniş konsentrasiya intervalında qarşılıqlı təsirdə olan komponentlərin tərkiblərinin və temperaturlarının qiymətlərini hesablamaq olar. Göstərilmişdir ki, işlənmiş bu tənliyin həlli ilə müəyyən temperatur intervalında maddənin halının dəyişməsini səciyyələndirmək mümkündür.

Ч.И. Абилов, С.А. Зейналов

УРАВНЕНИЕ ЛИНИИ ЛИКВИДУСА ФАЗОВОЙ ДИАГРАММЫ СИСТЕМЫ In_2Te_3-Co_3Te_4

Установлено уравнение для расчета линии ликвидуса диаграммы состояния системы In_2Te_3-Co_3Te_4. С этой целью, линия ликвидуса, состоящая из двух ветвей, была принята подобной ветвям двух парабол, отчего и для вывода математического выражения использованы уравнения параболы. Используя предложенное уравнение можно с высокой точностью рассчитать значения состава и температуры плавления взаимодействующих компонентов в широком концентрационном интервале.

Received: 05.03.02

METHOD AND TECHNICAL SOLUTIONS OF INFORMATIVITY INCREASE OF ACTINOMETRIC MEASUREMENTS

F.I. ISMAILOV

Azerbaijan National Aerospace Agency Institute of Ecology
370106 Baku, Azadlig avn. 159

The interpretation of actinometric information is considered as a parametric task of the analysis of the brightness components of the sky. With the purpose of its adequate solution, the constructive elements of spectrometers are proposed for manufacture of actinometric devices, realization and processing of measurement data in the course of natural experiments.

INTRODUCTION

Actinometric measurements allow to receive the most capacious information on optic conditions of the atmosphere in view of their regularity. At the same time there are some certain difficulties at one - valued interpretation of measurement data, mainly, because of obstacles of Forbs effect and optic instability of the atmosphere [1, 2].

At present at solution of these tasks, mainly in the field of ecological and climatological monitoring, there is a necessity of increase of exact actinometric information. It is connected with the possibility of research of space - time changeability and spectral structure of components of the day - time brightness of the sky.

This work proposes methods of unification of elements of actinometrics and the spectrophotometrics with the purpose of corresponding research on field brightness of a light radiation of the firmament, collection and treatment of actinometric information during realization of natural experiments.

SYSTEMATIC APPROACH

At research of the glow of the firmament the observed brightness is presented as a sum of additive components [2,4].

This allows to get various relationships, expressing the interrelation of consisting components of brightness of the sky.

The forming process of the field of glow radiation of firmament [3] is represented in the form of the diagramm on fig 1.

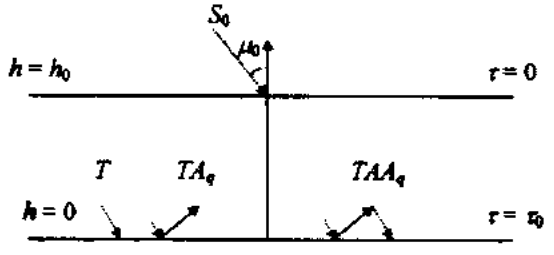

Fig. 1. The diagram of the forming of the glow radiation field of firmament.

Here h is the height, τ is the optic thickness of the atmosphere, S_0 is the solar constant; $\mu_0=\cos\theta_0$ where θ_0 is the angle of incidence of the direct radiation, T is the transmission, A is the albedo of the atmosphere, A_q is the albedo of the land surface.

The atmospheric transmission can be written as

$$T=\frac{F}{\mu_0 S_0}=T_D+p^{m}, \qquad (1)$$

where F is the incident radiation flux, T_D is the transmission for scattered radiation, $P=exp(-\tau)$ is the atmosphere transmittance, m_0 is the optic mass of atmosphere (for $\theta_0>30°$: $m_0=\sec\theta_0$ [1]).

Let's consider methods of analysis of nature characteristics p and T. On the input of the optic device the illumination S is determined according to formula [5]

$$S=\pi B\sin^2\varepsilon, \qquad (2)$$

where B is the brightness of the incident radiation, ε is the aperture angle in the space of objects.

Proportionality of values is supposed at calculations of the transparency of atmosphere:

$$\frac{S}{S_0}=\frac{F}{\mu_0 S_0} \qquad (3)$$

Atmospheric transparency is investigated in accordance with the Buger curve [1]

$$\ln\pi B_d=\ln S_d+m_0\ln p, \qquad (4)$$

where B_d is the brighuness of the direct radiation.

Solution of the task on brightness of the day - time sky we will carry out in accordance with fig 1. We try to differ the repeated scattering of coming solar radiation, determined by the transmission T, and multiple reflection in the system of "atmosphere - layer of the surface" determined by the product AA_q.

In atmospheric windows of transparency, at neglect of absorption, one may think that $A=1-T$. Thus at certain values of the independent parameter A_q the indicated task reduces to determination of the transmission T.

We can present the brightness of coming radiation as the sum:

$$B_t=B_s+B_m \qquad (5)$$

where B_s is the brightness of single scattering and B_m is the brightness of multiple scattering, B_t is the brightness of total scattering.

Component B_s is most simply calculated in almucantar of the Sun (in points of the firmament system with the same zenith distance as the Sun) [2].

$$B_s = S_0 f(\theta) p^{m_\oplus} m_\oplus . \qquad (6)$$

where $f(\theta)$ is the indicatrix of scattering of atmosphere; θ is the angle of scattering.

Observations show that following relationship takes place in the almucant ar of the Sun

$$B_m = const\, B_s . \qquad (7)$$

Here the proportionality coefficient is of the order of ÷0.13 in accordance with theoretical assessment.

ELEMENTS OF APPARATUS COMPLEX

The above mentioned systematic approach is based on measurement of brightness of direct radiation, single scattered radiation in almucantar of the Sun, multiple scattered radiation in "atmosphere - land surface" system.

Measurements and processing of data are carried out in the course of natural experiments. The fig. 2 shows the block - diagram of measuring apparatus.

Measurements are carried out in the window of atmosphere transparency. For this purpose the disk cassettes are used with replaced glass light filters due to their stability during a long - time exploitation.

Filters are installed in the optic system uniting blends 1, 2, objectives 4, light guides 6, condensers 5, 7, 9. Blend 1 with diaphragms serves for receiving of direct or single scattered radiation, and blend 2 with shaded enclosure serves for receiving of multiple scattered radiation. Enclosure 3 is mobile and is used for vignetting of stream of a scattered radiation. Set of condensers is necessary for collecting, averaging and direction of a light stream along the axis of the optic system. It is important because light guides and photodiodes with small area of the receiving surface are used. Amplifier 11 is assembled on low - voltage combined microscheme for guarantee of the temperature stability and application of the low power feeding source (12).

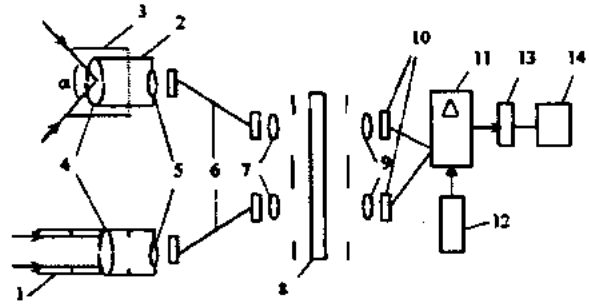

Fig. 2. Block - diagram of the measuring complex: 1, 2 are blends; 3 is the cylindrical enclosure; 4 are objectives; 5, 7, 9 are condenser lenses; 6 are light guides; 8 are cassettes with filters; 10 are photodiodes; 11 is the amplifier; 12 is the battery of amplifier feeding; 13 is the converter; 14 is the registration system.

Photo current is delivered to the personal ECM on lines of communication by means of converter (13).

Let's compare the characteristics of sensitivity of the optic system in fig. 2 by means of the table, using FD - 256 with actinometer and pyranometer. Because of low values of passage of optic systems the increase of sensitivity of all measuring system is supplied as a result of following factors:

1) equalization in accordance with fixing of sizes of lens blends 1, 2 with photo sensitive area of actinometer and pyranometer ;

2) use of the amplifier with no less than ten times magnification at the conservation of its temperature stability.

Table of comparison of sensitivity of optic system blends 1, 2, actinometer and pyranometer

Receiver	Integral sensitivity $\frac{mA}{Wt \cdot cm^2}$	Photo sensitivity area, cm^2	Transmittance of optic system	Diameter of input pupil, mm
Actinometer	4	5.3		38
Pyranometer	7	4		11
Optic system 1. Blends 1 2. Blends 2	9 (λ = (0.4 ÷ 1.1) mcm)	$1.5 \cdot 10^{-2}$	0.3 - 0.5	11 19

CONCLUSION

1. The systematic base of actinometric measurements of spectral brightness of the firmament is developed.

2. The problems of realization of complex actinometric measurements are considered.

3. Constructive elements of spectrophotometers for elaboration of actinometric apparatus are proposed.

[1] G.P. Guchin. Methods, instrumentation and results of atmospheric spectral measurements. L.: Gidrometeoizdat, 1988, p. 32 (in Russian).

[2] V.A. Glushkov, A.I. Ivanov, G.Sh. Livshitz, A.I. Fedulin. Alma - Ata, Izd-vo "Nauka", 1974, p. 480 (in Russian).

[3] F.I. Ismailov. Parameterization of effects of light scattering by submicronic aerozol. Baku, 1992, Cand. dis., p. 103 - 108. (in Russian).

[4] C.O. Oluwafemi. Pure Appl. Geophys., 1980, v. 118, ¹ 3, p. 775 - 782.

[5] Reference book of designer of optical-mechanical devices. L.: Mashinostroyenie, 1980, p. 86. (in Russian).

METHOD AND TECHNICAL SOLUTIONS OF INFORMATIVITY INCREASE OF ACTINOMETRIC MEASUREMENTS

F.İ. İsmayılov

AKTİNOMETRİK ÖLÇMƏLƏRİN İNFORMATİVLİYİNİN ARTIRILMASI METODİKASI VƏ TEXNİKİ HƏLLİ

İşdə aktinometrik məlumatların izahına səmanın parlaqlıq komponentləri arasındakı parametrik asılılığın analizi kimi baxılır. Məsələnin adekvat olaraq həll edilməsi üçün aktinometrik cihazların hazırlanmasında spektrometrlərin konstruktiv elementlərini istifadə edilməsi, ölçmələr toplusunun tədqiqatlar zamanı işlənməsi tövsiyə olunur.

Ф.И. Исмайлов

МЕТОДИКА И ТЕХНИЧЕСКИЕ РЕШЕНИЯ ПОВЫШЕНИЯ ИНФОРМАТИВНОСТИ АКТИНОМЕТРИЧЕСКИХ ИЗМЕРЕНИЙ

Интерпретация актинометрической информации рассматривается как параметрическая задача анализа компонент яркости небосвода. С целью ее адекватного решения предлагается использовать конструктивные элементы спектрометров для изготовления актинометрических приборов, проведение и обработку массива данных измерений в ходе натурных экспериментов.

Received: 15.03.02